High-pressure mechanochemistry: Conceptual multiscale theory and interpretation of experiments

Valery I. Levitas*
Texas Tech University, Center for Mechanochemistry and Synthesis of New Materials, Department of Mechanical Engineering, Lubbock, Texas 79409-1021, USA
(Received 30 May 2003; revised manuscript received 26 August 2004; published 19 November 2004)

Fifteen mechanochemical phenomena observed under compression and plastic shear of materials in a rotational diamond anvil cell (RDAC) are systematized. They are related to strain-induced structural changes (SCs) under high pressure, including phase transformations (PTs) and chemical reactions. A simple, three-scale continuum thermodynamic theory and closed-form solutions are developed which explain these phenomena. At the nanoscale, a model for strain-induced nucleation at the tip of a dislocation pile-up is suggested and studied. At the microscale, a simple strain-controlled kinetic equation for the strain-induced SCs is thermodynamically derived. A macroscale model for plastic flow and strain-induced SCs in RDAC is developed. These models explain why and how the superposition of plastic shear on high pressure leads to (a) a significant (by a factor of 3–5) reduction of the SC pressure, (b) reduction (up to zero) of pressure hysteresis, (c) the appearance of new phases, especially strong phases, which were not obtained without shear, (d) strain-controlled (rather than time-controlled) kinetics, or (e) the acceleration of kinetics without changes in the PT pressure. Also, an explanation was obtained as to why a nonreacting matrix with a yield stress higher (lower) than that for reagents significantly accelerates (slows down) the reactions. Some methods of characterization and controlling the SCs are suggested and the unique potential of plastic straining to produce high-strength metastable phases is predicted.

DOI: 10.1103/PhysRevB.70.184118 PACS number(s): 64.60.−i, 46.35.+z, 64.70.Kb

I. INTRODUCTION

Mechanochemistry studies the effect of nonhydrostatic stresses and plastic strains on various structural changes (SCs), which include chemical reactions (CRs) and phase transformations (PTs). SCs under high pressure and plastic shear are widespread in nature (e.g., in geophysics), physical experiments, and modern technologies. In particular, one of the mechanisms of deep earthquakes is related to the instability caused by shear strain-induced PT.[1] Shear ignition of energetic materials[2,3] is subject to intensive study with the goal to assess safety issues. Mechanosynthesis (or mechanical alloying), i.e., strain-induced synthesis of various chemical compounds by ball milling, is another example.[4] We also mention the importance of mechanochemical processes for understanding friction and wear, shear-induced metallization, and oxidation. The most fundamental results in strain-induced SCs were obtained in a rotational diamond anvil cell (RDAC) (Fig. 1). After compression of the materials in RDAC, a very high pressure is produced in the center of the specimen, which leads to a number of SCs. It is known from numerous experiments that the addition of plastic shear, due to the rotation of an anvil, leads to findings that have both fundamental and applied importance. In particular, it leads to (a) a significant (by a factor of 3–5) reduction of SC pressure and pressure hysteresis, (b) an appearance of new phases, (c) a substitution of a reversible PT by an irreversible PT, and (d) strain-controlled kinetics (see Sec. II). Grinfeld[5] assumes that acceleration of CR is caused by rapid corrugation of reaction interfaces triggered by the shear stress driven rearrangement instabilities. Gilman[6] suggests that *elastic* shear strain can accelerate CR by lowering the highest occupied bonding–lowest unoccupied antibonding molecular orbital energy gap. However, in RDAC, SCs do not occur without *plastic* shear despite the fact that the friction shear stress and consequently elastic shear of the same magnitude are present at compression without or after anvil rotation. Some other ideas are presented in Refs. 7 and 8. However, *there has not been any theory describing thermodynamic and kinetic coupling between plasticity and SC and any one of the above experimental effects*. In Ref. 9, the *macroscopic* theory of plastic flow in the sample was developed, which explains qualitatively some of the above phenomena. One of the noteworthy confirmations of our approach is that of obtaining an irreversible PT from rhombohedral rBN to superhard cubic cBN at a low pressure of 5.6 GPa, instead of 55 GPa under hydrostatic conditions.[10,11] More quantitative analysis, however, shows that a macroscopic approach is not sufficient for the explanation of the above phenomena, even at the order-of-magnitude accuracy.

In this paper, we developed a *multiscale continuum thermodynamic and kinetic* theory which explains the key phenomena occurring during *strain-induced SCs* under high pressure and allows us to develop a *new characterization* of PT and CR under plastic deformation, as well as *methods of control of SCs*. The theory is based on a general theory of SCs in plastic materials, which we developed in Refs. 9 and 12 (see Sec. III), and closed-form solutions for stress and strain fields that we found. We believe that our models will be applicable for various materials and loadings. This belief is supported by results described in item 14 (Sec. II). At the nanoscale (Sec. IV), the main reason for the above phenomena is related to the *strain-induced* rather than pressure- or stress-induced SCs. Strain-induced SC occurs by nucleation

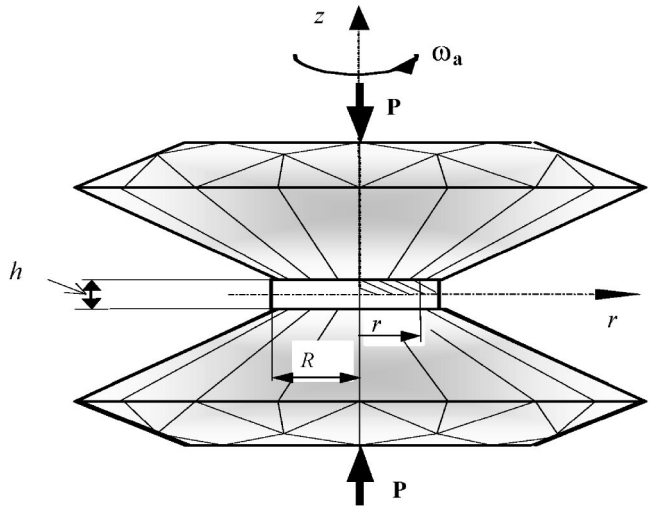

FIG. 1. The scheme of compression and shear of materials in a rotational diamond anvil cell. Material is compressed by an axial force, P, followed by the rotation of one of the anvils with an angular velocity, ω_a.

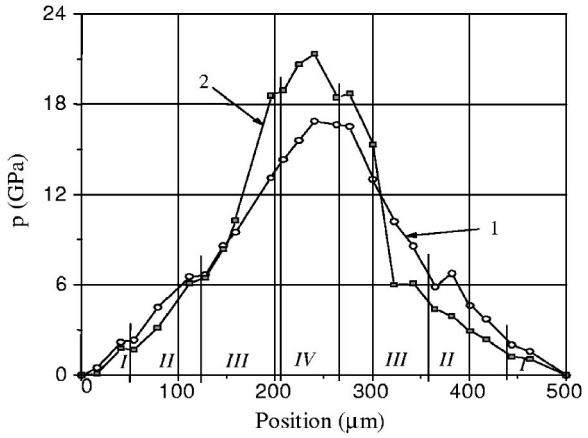

FIG. 2. Radial pressure profiles in a fullerene sample before (1) and after (2) a shear strain (Ref. 20).

on new defects generated by plastic flow which produce strong stress concentrations. We developed a model of nucleation at the tip of the dislocation pile-up. It can also be approximately applied to nucleation at strain-induced tilt boundary, produced by intersection of slip bands, twins, and bundles of stacking faults, including intersection with grain boundaries. It is demonstrated that shear stress can lead to the substitution of thermally activated nucleation with barrierless nucleation and significantly reduce SC pressure for direct SC, as well as increase SC pressure for reverse SC. At the microscale (Sec. V), a new strain-controlled kinetic equation is developed which takes into account the possibility of direct and reverse SC and the difference in the plastic strain in each phase because of the different yield stress of the phases. The conditions for zero-pressure hysteresis were demonstrated. At the macroscale (Sec. VI), plastic flow and SC in RDAC are described. Changes in the SC conditions due to the rotation of the anvil are related to the possibility of additional axial displacement, which compensates for a volume decrease due to SC and increases pressure and plastic strain. The pressure self-multiplication effect is described. It is also obtained that the rotation of an anvil can lead to new phases, which were not obtained without the rotation of the anvil. These solutions predict the unique potential of the rotating anvil method to produce high-strength metastable phases. In Sec. VII, a method of experimental characterization of strain-induced SCs is substantiated. The difference between pressure- or stress-induced and strain-induced SCs, which is not appreciated by the high-pressure community, is discussed. It is shown that the only complete characterization of strain-induced SCs can be obtained with the help of a strain-controlled kinetic equation which parametrically depends on pressure; an example of such an equation is given in Sec. V. The possible experimental procedures are outlined. In Sec. VIII, a combination of nano-, micro-, and macroscale models is used to summarize the explanation and interpretation of 15 experimental phenomena described in Sec. II. In Sec. IX, our analysis of various examples which we considered is summarized as possible ways of controlling SCs by the purposeful control of the thermomechanical loading process and microstructure.

Direct tensor notations are used throughout this paper. Vectors and tensors are denoted in boldface type; $\boldsymbol{A}\cdot\boldsymbol{B}=(A_{ij}B_{jk})$ and $\boldsymbol{A}:\boldsymbol{B}=A_{ij}B_{ji}$ are the contraction of tensors over one and two nearest indices. The indices 1 and 2 denote the values before and after the SC, := means equals per definition, and $\boldsymbol{I}$ is the unit tensor.

II. EXPERIMENTAL PHENOMENA

Researches of PT and CR in rotational Bridgman anvils were reported in Refs. 8, 13, and 14. Blank *et al.* developed the RDAC and obtained a number of very interesting results, see Refs. 15–19. The mechanical aspects of material behavior in RDAC were analyzed in Ref. 20. Recently, experimental research using RDAC was initiated in the United States.[21] Below, we enumerate and systematize some experimental phenomena, which occur during the compression and shear of various materials in RDAC. These phenomena are important for the analysis of the effect of plastic strain on high-pressure SCs.

1. Plastic shear significantly reduces (by a factor of 3–5) SC pressure for some PTs (Refs. 15, 16, 18, and 20) and CRs.[8] At the same time,[22] for some PTs (calcite↔aragonite, quartz↔coesit) additional shear does not change the PT pressure at any temperature; however, it significantly accelerates PT kinetics.

2. Small "steps" (regions with almost constant pressure) are found at the very heterogeneous pressure distribution (Fig. 2).[16,18,20] These steps correspond to two-phase regions (diffuse interfaces) in which PT occurs. It is suggested that the pressure at these steps characterizes PT.[16,18] However, there is no theory supporting this hypothesis.

3. Plastic shear reduces pressure hysteresis, i.e., the difference Δp between the start pressure of direct and reverse PT,[15] in some cases to zero.[16] From this, it was claimed that the pressure at the diffuse interface under compression and

shear can be interpreted as an equilibrium pressure. As we will show below, this is not true.

4. For some PT [e.g., semiconductor→metal in InSb, InTe, Ge (I→II), and Si (I→II) (Ref. 15)], direct PT pressure under shear is lower than equilibrium pressure. It is also lower than the reverse PT pressure under hydrostatic conditions.

5. Plastic shear leads to new phases (materials) which were not produced without rotation. As examples, we can mention phase V of fullerene C_{60} (Fig. 2) (Refs. 16 and 20) (which is harder than diamond), the macromolecular products of methylmethakrylate and maleic anhydride, and others.[8,23]

6. Shear deformation substitutes a reversible PT with an irreversible PT, e.g., for PT graphite↔hexagonal diamond.[17] Consequently, the rotation of an anvil allows production of phases which are metastable at normal pressure and can be used in engineering applications. These results indicate that shear deformation increases pressure hysteresis, which is in contradiction with the results in item 3.

7. The volume fraction of the product phase is an increasing function of the rotation angle and consequently of the plastic shear strain. When the rotation stops, PT stops as well (see Ref. 15 for PT and Ref. 8 for CR). Therefore, a pressure-temperature-shear phase diagram is suggested[15,18] and strain-controlled kinetics is considered.

8. The rate of solid-state CR increases by a factor of 10^2-10^5 with shear strain compared with liquid-phase CR, e.g., for some polymerization reactions in acrylamide, styrene, and butadiene.[8] Heating due to plastic flow is not significant and the existence of hot spots where the material is melted cannot explain high rates of CR.[8]

9. Sometimes, under rotation of an anvil under a fixed compressive force, the pressure grows in the transforming region despite the volume decrease due to PT.[16,18,20] This is the so-called "pressure self-multiplication effect" (Fig. 2), which represents a violation of the Le Shatelie principle. At the same time, the pressure reduces for PT III→II in Ge under shear.[15,18]

10. The rate constant for CR in organic compounds in the presence of an indifferent (nonreacting) matrix depends linearly on the yield stress of the matrix.[8] A matrix with the yield stress higher (lower) than that for reagents accelerates (slows down) the CR.

11. An increase in deformation rate reduces PT pressure for PT in InSb,[15] KCL, and RbCl (Ref. 24) and accelerates decomposition of some oxides.[14] It does not affect the volume fraction of the polymer produced.[8]

12. Plastic straining changes the transformation path.[15,18] For example, it causes I→III→II PT instead of I→II for PTs in Ge and Si.[15,18]

13. Pressure hysteresis for PT after preliminary plastic deformation is proportional to the material hardness and consequently the yield stress.[9,12,24]

14. Regardless of the method used for creating the high pressure and shear deformation conditions (rotating anvils, shock wave, extrusion, extrusion through an annual gap with simultaneous rotation of dorn), the same reactions occur which do not occur at the usual compression up to a pressure of 8 GPa.[8]

15. Without PT, pressure distribution is practically independent of rotation[16,20] and of the complex deformation history.[20]

More detailed description of the above phenomena can be found in Ref. 25. There are a number of problems which we would like to address in this paper. What are the main reasons for the above effects and some of the above contradictions? Is it possible to define the equilibrium pressure in experiment using the RDAC technique? How do we characterize and describe high-pressure SC under plastic straining? Is the pressure-temperature-shear diagram informative? The goals of this paper are (a) to develop a first conceptual three-scale theory for strain-induced SC and apply it to explain in first approximation the above phenomena; (b) to apply this theory for the interpretation of measurement of SC pressure and the characterization of strain-induced SCs under high pressure; (c) to find and systematize possible methods to control the SCs which can be used in physical experiments and engineering practice; (d) to outline new coupled theoretical, experimental, and modeling problems based on new understanding gained from the developed theory.

Ultimately, it is necessary to develop a theory which will allow computational modeling of strain-induced SCs and comparison of SCs in various high-pressure apparatuses and various loadings. Consideration at the nanoscale will be done for crystalline solids. Microscale and macroscopic treatments can be applied, probably for any material. The fact that the above phenomena are observed for various PTs and CRs in various classes of materials suggests that there are some *universal microscopic (at the scale of* $1-1000$ μm*) and macroscopic (at the scale of the sample) reasons for them, independent of specific atomistic and nanoscale mechanisms of SC and material system*. For convenience, compressive stress (pressure) and strains will be considered as positive. Reference to "item 3" means item 3 in Sec. II.

III. NET DRIVING FORCE FOR STRUCTURAL CHANGES IN INELASTIC MATERIAL

As a main geometrical characteristic of the SCs, we consider transformation strain. For martensitic PT, transformation strain, $\boldsymbol{\varepsilon}_t$, transforms a crystal lattice of parent phase (austenite) into a crystal lattice of product phase (martensite). For solid-solid SCs, including reconstructive PTs and CRs, $\boldsymbol{\varepsilon}_t$ transforms an infinitesimal volume or unit cell of the stress-free parent phase into an infinitesimal volume of the stress-free product phase. In the case of CR, both materials, before and after the CR, can consist of several substances. For brevity, we will use the term "phases" in this case as well. We neglect all internal atomic displacements (e.g., shuffles) inside the volume under consideration, even if they represent the primary (i.e., responsible for material instability) order parameters and $\boldsymbol{\varepsilon}_t$ is the secondary (induced) order parameter. The stress tensor does not produce work on these displacements and we assume that they are expressed in terms of $\boldsymbol{\varepsilon}_t$ by energy minimization.[26] This is the usual practice in thermodynamic study of reconstructive fcc→bcc and fcc →hcp PTs in ferrous and transition-metal alloys.[27] This is also similar to classical thermodynamics of hydrostatically

loaded solids; when independent of the type of SCs, pressure produces work on volume change. In our approach, the stress tensor $\boldsymbol{T}$ produces work on the transformation strain tensor. We define the SC as a thermomechanical deformation process of growth of transformation strain $\boldsymbol{\varepsilon}_t$ from $\boldsymbol{\varepsilon}_{t1}$ in the initial phase to the final value $\boldsymbol{\varepsilon}_{t2}$ in the product phase, which is accompanied by a jump in all the thermomechanical properties. For the description of SC in an elastic solid, the principle of a minimum of Gibbs free energy is usually used. For inelastic materials, a corresponding principle has been lacking. It was necessary to develop a conceptually new approach and to verify it by explanation and interpretation of a number of experimental phenomena. A general thermomechanical theory of SCs in inelastic materials, developed by the author, is presented in Ref. 12 and references therein; see also the review in Ref. 25. It was applied to find a number of analytical and numerical solutions which were used for interpretation of experiments. They, in particular, include the following: SCs in spherical inclusion with application to graphite-diamond PT (Refs. 9 and 12); PTs and CRs in shear band with the revealing reaction-induced plasticity (RIP) phenomenon;[3,12] interaction between PT, semicoherence and fracture;[28] strain-induced nucleation at the shear-band intersection in TRIP steel;[29] appearance and growth of a small temperature-induced martensitic plate with application to the plate-lath morphological transition in steel;[28,30] and low pressure PT $rBN \rightarrow cBN$ and revealing PT induced by the rotational plastic instability phenomenon.[10]

We will only use the simplest form of equations necessary for our study. To avoid unnecessary complications, we will use a small strain formulation. Finite strain theory and some analytical and numerical solutions can be found in Refs. 12, 25, and 30. Our experience shows that allowing for finite strain does not change conceptual conclusions, which are the main goal of this work. We need to describe very strong effects, which allows us to neglect all second-order contributions. In the simplest case, when the temperature θ is fixed and homogeneous in a transforming volume and elastic properties of phases are the same, the net thermodynamic driving force for SC in the region V_n bounded by surface Σ is as follows:[12]

$$F := (X-K)V_n = \int_{V_n}\int_0^{\boldsymbol{\varepsilon}_{t2}} \boldsymbol{T}:d\boldsymbol{\varepsilon}_t dV_n - [\Delta\psi(\theta)+K]V_n - \int_\Sigma \Gamma d\Sigma. \quad (1)$$

Here X is the driving force for SC, which represents the total calculated dissipation increment due to SC only (i.e., excluding all other types of dissipation, e.g., plastic dissipation) during the entire transformation process, averaged over the transforming region; K is the athermal dissipation due to SC related mostly to interface friction; $\Delta\psi$ is the jump in the thermal part of the Helmholtz energy; and Γ is the surface energy. The key point of Eq. (1) is that it takes into account the whole history of stress variation during the transformation process, which depends, in particular, on the interaction of the transforming region with the surrounding material. This may ilustrate that the PT pressure obtained not only in different high-pressure apparatuses but also in the same apparatus under different conditions (e.g., geometry and properties of a gasket) differs significantly. Another important point is that the driving force (1) takes into account the stress tensor rather than the pressure only. For elastic materials, the expression for XV_n coincides with the change in Gibbs free energy of the whole system,[12] i.e., like in a standard approach. The value K can be different at different scales, and it seems to be a very complex functional of the thermomechanical deformation process and the material microstructure. However, at the macroscale, we found[9,12] the surprisingly simple formula

$$K = L\sigma_y\varepsilon_o, \quad (2)$$

where σ_y is the yield stress, ε_o is the volumetric transformation strain, and L is the coefficient given for some materials in Refs. 9 and 12. Thus, preliminary plastic deformation, increasing σ_y due to strain hardening, suppresses SCs. There are a lot of sources of dissipation K due to SC. These include interaction of a moving interface with various defects, e.g., point defects (solute and impurity atoms, vacancies), dislocations, grain, subgrain, and twin boundaries; precipitates; and the Peierls barrier. The parameter K characterizes an interaction of moving interface and material microstructure, and σ_y is an integral characteristic of microstructure because plastic flow represents motion of dislocations through the same obstacles.

IV. NANOSCALE STUDY

Stress- and pressure-induced SCs occur predominantly by nucleation at existing defects when external stresses do not exceed the macroscopic yield limit σ_y. Strain-induced SC occurs by nucleation at new defects generated during plastic flow. In metals, strain-induced PTs at normal pressure occur at strain-induced tilt boundaries, produced by the intersection of slip bands, twins, and bundles of stacking faults, including intersection with grain boundaries.[27] We are not aware of any experimental or theoretical work for materials compressed and sheared in diamond anvils that (a) determines the nucleating defects, (b) describes theoretically its effect on nucleation, and (c) tries to describe phenomena enumerated in Sec. II. The lack of specific models does not allow one to analyze whether this is sufficient for such a strong effect of plastic strain on SC pressure and for explanation of some other above-mentioned phenomena. It is also unclear which and how material and loading parameters affect the above phenomena.

Let us consider one possible mechanism of intensification of SC by the stress concentration created by dislocation pile-up. Dislocation pile-up is considered as a strong defect used to model slip transfer from grain to grain,[31] temperature-induced martensitic PT,[32] and deformation twinning.[33] The importance of dislocation mechanisms for CR is discussed in Refs. 2 and 8. Our model has some distinctions and will allow us to analyze the effect of shear stress on SC pressure and kinetics. Transition from thermally activated to barrierless nucleation at some level of shear stresses is revealed. For an explanation of the reduction of SC pressure by a factor of 3–5, the strongest defect is required, such as pile-up

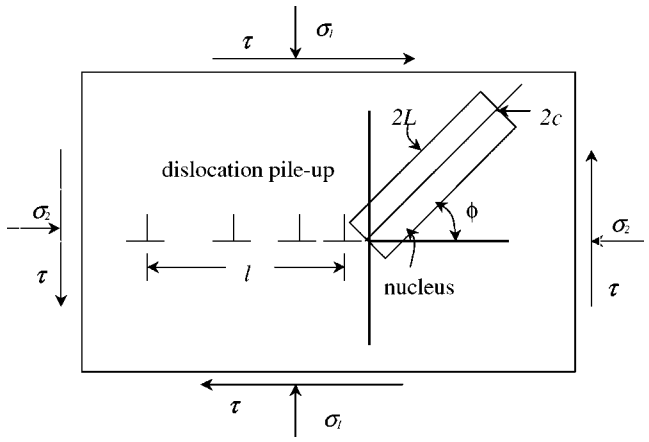

FIG. 3. The nucleation scheme at the tip of dislocation pile-up.

consisting of ~20 dislocations (see the estimate below). If the dislocation pile-up would not be able to explain such an effect, none of the other defects could help and new physics would be required. However, we do not exclude that for some materials with the weaker effect of shear stress on SC pressure, other defects (grain and subgrain boundaries, twins, and stacking faults) may be more important. The dislocation pile-up is approximated in this paper by superdislocation. Since tilt boundary is approximated in Ref. 27 by superdislocation as well (for temperature-induced PTs), our analysis can be approximately applicable to strain-induced tilt boundaries mentioned above. Note that under high pressure, even brittle materials can undergo large plastic deformations by a dislocation mechanism, thus our model is also applicable to them.

Nucleation at dislocation pile-up: Analytical solution. Assume that plastic flow occurs by activation of Frank-Read or Köehler sources and motion of generated edge dislocations to a barrier (e.g., grain boundary, twin or subgrain boundary, or slip band). Dislocation pile-up of length l assists in nucleating of the second phase region. A nucleus will be considered as a pill box with sizes $2L\times 2c\times b$, with $n=c/L\ll 1$ (Fig. 3), inclined under angle ϕ in the pile-up direction. A pill-box shape is a reasonable approximation to a solution based on the phase field model for temperature-induced PTs.[32] Plane stress formulation will be used. Transformation strain $\boldsymbol{\varepsilon}_t$ in the nucleus is an invariant plane strain consisting of shears, 0.5γ, along the sides L and c (due to symmetry of $\boldsymbol{\varepsilon}_t$), and normal strain, ε, along side c. Allowing for other components of transformation strain is trivial and does not change our main conclusions. External stresses have normal, σ_1 and σ_2, and shear, τ, components, where τ is the resolved shear stress for dislocation motion, i.e., the yield stress in shear τ_y. To estimate the driving force, one has to calculate the transformation work

$$A_t=\int_{V_n}\int_{\mathbf{0}}^{\boldsymbol{\varepsilon}_t}\boldsymbol{T}:d\tilde{\boldsymbol{\varepsilon}}_t dV_n,\quad \boldsymbol{T}=\boldsymbol{\sigma}+\boldsymbol{\sigma}_{es}+\boldsymbol{\sigma}_d, \tag{3}$$

where $\boldsymbol{\sigma}$, $\boldsymbol{\sigma}_{es}$, and $\boldsymbol{\sigma}_d$ are the contributions to total stress $\boldsymbol{T}$ from external stress, internal stresses due to ε_t (Eshelby inclusion stress), and dislocation pile-up, respectively. Stresses $\boldsymbol{\sigma}$ and $\boldsymbol{\sigma}_d$ are independent of $\boldsymbol{\varepsilon}_t$. For the external stress, the Mohr transformation is used. The work of $\boldsymbol{\sigma}_{es}$ is estimated for an ellipsoidal cylinder of infinite length with semiaxes L and c. We have[34] $\sigma_{es}=-\mu n\tilde{\varepsilon}/(1-\nu)$, $\tau_{es}=-\mu n\tilde{\gamma}/(1-\nu)$, and

$$\int_{V_n}\int_{\mathbf{0}}^{\boldsymbol{\varepsilon}_t}\boldsymbol{\sigma}_{es}:d\tilde{\boldsymbol{\varepsilon}}_t dV_n=\pi Lcb\left(\int_0^{\varepsilon}\sigma_{es}d\tilde{\varepsilon}+\int_0^{\gamma}\tau_{es}d\tilde{\gamma}\right)$$
$$=-4bn^2L^2s(\varepsilon^2+\gamma^2), \tag{4}$$

where $s=\mu\pi/[8(1-\nu)]$, and μ and ν are the shear modulus and Poisson ratio, respectively. The stress field of the pile-up will be approximated by the stress field of superdislocation,[31]

$$\sigma=\frac{l\tau}{2}\frac{\sin\phi}{r},\quad \tau_l=\frac{l\tau}{2}\frac{\cos\phi}{r}, \tag{5}$$

where r is the current radius of the points of nucleus (measured from the pile-up tip), and τ_l and σ are the shear and normal stresses along sides L and c. Note that stresses

$$l\tau=\mu N|\boldsymbol{b}|/[\pi(1-\nu)] \tag{6}$$

are proportional to the number N of dislocations in a pile-up (and approximately to plastic strain), i.e., they can be extremely high.[31] Here $\boldsymbol{b}$ is the Burgers vector. We can estimate corresponding transformation work: $\int_{V_n}\int_{\mathbf{0}}^{\boldsymbol{\varepsilon}_t}\boldsymbol{\sigma}_d:d\boldsymbol{\varepsilon}_t dV_n=l\tau bLn\ln(2/n)(\varepsilon\sin\phi+\gamma\cos\phi)$, where the cutoff radius of dislocation is taken as $c>|\boldsymbol{b}|$, which underestimates the transformation work. Substitution of pile-up with a superdislocation also reduces stresses and transformation work for $r>|\boldsymbol{b}|$. Finally, one obtains

$$F=\{[0.5(\sigma_1+\sigma_2)+0.5(\sigma_1-\sigma_2)\cos 2\phi+\tau\sin 2\phi]\varepsilon+[0.5(\sigma_2-\sigma_1)\sin 2\phi+\tau\cos 2\phi]\gamma\}4bnL^2$$
$$-(\Delta\psi+K)4bnL^2-4bn^2L^2s(\varepsilon^2+\gamma^2)+l\tau bL(\varepsilon\sin\phi+\gamma\cos\phi)n\ln 2/n-4\Gamma L(b+bn+2nL). \tag{7}$$

According to the postulate of realizability,[9,12] the net driving force has to be maximized with respect to ϕ and n, which is impossible to do analytically. We first maximize it with respect to ϕ for the case when contribution from the pile-up is much stronger than from the external stresses, i.e., by varying ϕ in the pile-up term only. Then one obtains from Eq. (7)

$$\tan\phi = \varepsilon/\gamma;\quad F = AL^2 + BL;$$

$$B = l\tau b\sqrt{\varepsilon^2+\gamma^2}n\ln 2/n - 4\Gamma b,$$

$$A = (\sigma_2\varepsilon + \tau\gamma)4bn - (\Delta\psi + K)4bn - 4bn^2 s(\varepsilon^2+\gamma^2) - 8\Gamma n. \tag{8}$$

This also gives us the lower bound for F. If $B<0$, which is the case for the weak or no dislocation pile-up and low τ, nucleation requires thermal fluctuations (see Sec. IV B.). We start with the case $B>0$.

A. Barrierless nucleation

If $B>0$, which is true for the strong dislocation pile-up and large τ, even for $A<0$ for relatively small L, one has $F>0$. That shows that barrierless nucleation occurs independent of the magnitude of A and pressure. However, the equilibrium value of $L_e=-B/A$, determined from the condition $F=0$, depends on A. We can maximize B with respect to n, however the obtained value $n=2/e=0.74$ does not satisfy the condition $n\ll 1$, which was used in the above derivations. We assume $n=0.1$ as the maximum reasonable value satisfying this condition. Then the criterion for barrierless nucleation, $B>0$, is $l\tau > 13.35\Gamma/\sqrt{\varepsilon^2+\gamma^2}$. If we take $\Gamma=0.1$ N/m (a typical value for a semicoherent interface for steels), $\varepsilon=0.1$, and $\gamma=0.2$, then $l\tau>5.97$ N/m. This condition can be easily satisfied for reasonable values of τ and l, e.g., $\tau=0.1$ GPa, $l=60$ nm or $l=1$ μm, and $\tau=6$ MPa. For the coherent nucleus for ferrous and nonferrous alloys, $\Gamma=0.01$ N/m, which makes barrierless nucleation even easier. Alternatively, we can estimate the number of dislocations N necessary for barrierless nucleation by using Eqs. (6): $N>13.35[\Gamma\pi(1-\nu)]/(\mu|\boldsymbol{b}|\sqrt{\varepsilon^2+\gamma^2})$. If, in addition to the above parameters, we chose $|\boldsymbol{b}|=3\times10^{-10}$ m and $\nu=0.3$, then N dislocations will lead to barrierless nucleation for $\mu \geqslant 43.76/\mathrm{N}$ GPa. Consequently, the thermally activated regime is important for materials with relatively low elastic moduli, small $\boldsymbol{\varepsilon}_t$, and $\boldsymbol{b}$. Let us define the effect of shear stress on SC pressure for the appearance of a nucleus of a detectable size L at $\sigma_1=\sigma_2=p$. From condition $L=-B/A$, one derives

$$p = \frac{\Gamma}{\varepsilon}\left(\frac{2}{b}+\frac{1}{nL}\right) + \frac{\Delta\psi + K + ns(\varepsilon^2+\gamma^2)}{\varepsilon} - \tau\left[\frac{\gamma}{\varepsilon} + \frac{1}{4}\sqrt{1+\left(\frac{\gamma}{\varepsilon}\right)^2}\frac{l}{L}\ln\frac{2}{n}\right]. \tag{9}$$

The larger b is, the larger will be the driving force for nucleation and the smaller will be the SC pressure. One has to choose the maximum possible b, which is the length of dislocation in the b direction. The main parameter which determines the reduction of SC pressure due to τ is l/L. The characteristic size of the strain-induced unit in steel is 100 nm,[27,29] so $L=50$ nm. The parameter l depends significantly on microstructure and is limited, approximately, by a quarter of the grain size. If we take $l=1$ to 10 μm, then $l/L=20$ to 200. In this case, the effect of macroscopic shear stress is negligible in comparison with the effect of dislocation pile-up, and the SC pressure can be reduced significantly.

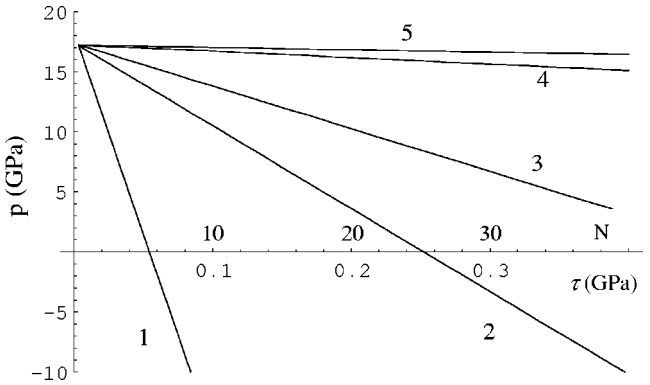

FIG. 4. Dependence of SC pressure on shear stress and number of dislocations for athermal nucleation at dislocation pile-up for the pile-up length $l=10^{-6}$ m and various nucleus length $2L$: 1, $2L=10^{-8}$ m; 2, $2L=10^{-7}$ m; 3, $2L=5\times10^{-7}$ m; 4, $2L=10^{-6}$ m; 5, $2L=\infty$.

Analysis and interpretation of experimental phenomena

We estimate this effect for the above values of ε, γ, ν, Γ, n, and $\Delta\psi=1$ GPa, $K=0.5$ GPa, $\mu=80$ GPa, $b=10^{-6}$ m. Then $p=17.24+10^{-8}/L-(2+1.675l/L)\tau$ (GPa). Dependence $p(\tau)$ for $l=10^{-6}$ m and various L is shown in Fig. 4. Because the term $10^{-8}/L$ is negligible for the L of interest, the relationship in Fig. 4 can be considered as a function of l/L. The larger the nucleus is, the smaller the effect of pile-up and shear stresses. For an infinite nucleus ($A=0$), we have $p=17.24-2\tau$. For $2L=50$ nm and $l=10^3$ nm, Eq. (9) simplifies to $p=17.64-68.99\tau$ (GPa). For a minimal value $\tau=5.97\times10^{-3}$ GPa, determined from the condition $B=0$, one has $p=17.23$ GPa. For $\tau=0.2$ GPa, $p=3.84$ GPa, i.e., reduction of SC pressure by factor 3–5 and higher (item 1) can be justified using the above model. For $\tau=0.256$ GPa, $p=0$, which is essentially lower than the SC equilibrium pressure, $p_e=10$ GPa, and even the reverse SC pressure of 2.6 GPa under hydrostatic conditions (item 4). Using Eq. (6), we can estimate the effect of a number of dislocations in a pile-up on SC pressure: $p=17.64-1.828\times10^{-8}N/L$ (GPa), where L is in m. For $L=25\times10^{-9}$ m, one has $p=17.64-0.731N$ (GPa). Consequently, 25 dislocations in a pile-up can reduce the SC pressure to zero. For $L=10^{-7}$m, 100 dislocations are necessary, which is also not an exotic number. For data in Fig. 4, we obtain τ (GPa)$=0.0109N$, which allows us to express a SC pressure p versus N.

Barrierless nucleation, which does not require thermal fluctuations, explains the strain-controlled rather than time-controlled kinetics (item 7). Indeed, the prescribed strain increment generates dislocation pile-ups with barrierless, i.e., very fast, nucleation and growth of the product phase up to the length L_{eq}. For the observation time of 1 s, this looks like instantaneous SC. As straining stops, no new defects and nuclei appear, and the growth of existing nuclei is thermodynamically impossible. Pure hydrostatic pressure in homoge-

neous systems does not cause plastic flow and the appearance of strong stress concentrators, which explains the unique role of shear stress and strains on SC. Even for $\gamma=0$ (e.g., for isostructural, electronic PTs in Ce, and its alloys), i.e., when τ does not contribute to transformation work, Eq. (9) exhibits a significant effect of τ on p because of the pressure concentration at the tip of the pile-up [see Eq. (5)].

One of the conditions of applicability of the above model is that the dislocation pile-up does not activate alternative mechanisms of stress relaxation like dislocation slip, twinning, or fracture. This limits maximum τ by τ_r, necessary for the activation of alternative relaxation mechanisms, as well as l. Stress τ_r is not smaller than τ_y, which was taken into account in the range of τ in the above estimates. Pressure strongly suppresses fracture and moderately increases the critical stress for dislocation slip. That is why *mechanochemical effects are more pronounced under high pressure*. If only SC and dislocation slip compete, then any increase in strain rate has to promote the SC, similar to competition between slip and twinning.[33] For slip, higher shear stress is necessary for higher strain rate, which increases τ in Eqs. (9). Indeed, some experiments show significant reduction in PT and CR pressure under increased strain rate.[14,15,24] As the yield stress in shear τ is limited, there exists a lowest possible pressure, p_ε^d, below which strain-induced SC is impossible. Because length l is limited by the grain size, which significantly reduces during large plastic deformation, one way to intensify SC is related to the increase in grain size and l. This can be done by annealing and recrystallization after compression of the disk at pressures slightly lower than p_ε^d. On the other hand, reduction in grain size has to suppress strain-induced SC, which is the case for explosives.[2] An increase in σ_y (by increasing strain and strain rate) leads to a decrease in p_ε^d, which is observed experimentally.[14,15,24] Here and later, the subscripts d and r designate direct and reverse SC.

Note that dislocation pile-up generates both compressive ($\phi>0$) and tensile ($\phi<0$) pressure of the same magnitude. Consequently, it simultaneously promotes both direct and reverse SC in different regions. The same equations with tensile ε can be applied for the description of reverse SC. We will take the above results into account at the microscale.

B. Thermally activated nucleation

If $B<0$, which is the case for the weak or no dislocation pile-up and low τ, then SC is possible for $A>0$ only. Because $F<0$ for $L<-B/A$, nucleation requires thermal fluctuations. There is a critical length $L_c=-B/(2A)$ which is determined by the minimization of F (similar to the maximization of the Gibbs potential) and will be used to find an activation energy Q. Designate $\overline{B}=B/(4b)$, $A=ab-8\Gamma n$, with $a=(p\varepsilon+\tau\gamma-\Delta\psi-K)4n-n^2 4s(\varepsilon^2+\gamma^2)>0$. Substitution of $L_c=-B/(2A)$ in the equation for $Q=-F$ leads to $Q=4\overline{B}^2b^2/(ab-8\Gamma n)$. Minimizing Q with respect to b, one obtains $b=16\Gamma n/a$; $A=8\Gamma n$; $Q=128(\Gamma n\overline{B}^2/a^2)$. For the observable nucleation rate, it is usually assumed $Q=40k\theta$, where k is the Boltzmann constant. Solving this equation for p, one obtains

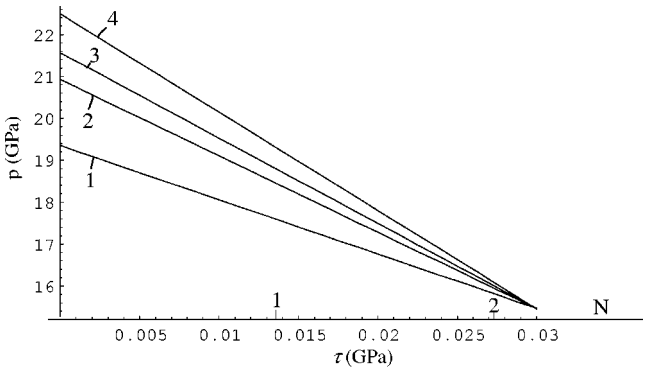

FIG. 5. Dependence of SC pressure on shear stress and number of dislocations for thermally activated nucleation at dislocation pile-up for the pile-up length $l=2\times10^{-7}$ m and various temperatures: 1, $\theta=1000$ K; 2, $\theta=500$ K; 3, $\theta=400$ K; 4, $\theta=300$ K.

$$p=\frac{\Delta\psi+K+ns(\varepsilon^2+\gamma^2)}{\varepsilon}+\frac{\Gamma}{\varepsilon}\sqrt{\frac{\Gamma}{5k\theta n}}-\tau\left\{\frac{\gamma}{\varepsilon}+0.25l\sqrt{\frac{\Gamma}{5k\theta n}\left[1+\left(\frac{\gamma}{\varepsilon}\right)^2\right]}n\ln\frac{2}{n}\right\}. \quad (10)$$

Substituting the same numbers as before (except $\mu=20$ GPa in order to have $N>2$ and $l=2\times10^{-7}$ m), one obtains the relationship $p(\tau)$ for various temperatures, see Fig. 5. Using Eq. (6), we obtain $\tau\,(\mathrm{GPa})=0.0136N$ and can estimate the effect of N on SC pressure. All plots intersect at the point corresponding to $B=0$ and barrierless nucleation. The smaller temperature is, the stronger the effect of shear stress is. If the term with γ/ε is negligible, SC pressure depends on τl. For $\theta=300$ K, one gets $p=22.5-234.8\tau$ (GPa). The effect of τ is much more pronounced for a thermally activated regime than for barrierless nucleation. However, because τ is limited by the condition $B\leqslant0$, the minimal pressure for thermally activated nucleation is 15.71 GPa.

For a thermally activated regime, i.e., for relatively weak defects, one has to take into account preexisting defects, because they can produce a comparable stress concentration. For example, they can be generated by preliminary thermomechanical treatment and are locked after unloading.[31] Dislocation pile-ups, observed at zero external stresses, are equilibrated by internal stresses τ_i, e.g., due to friction, misfit strain, or other defects. Using Eq. (6), one can estimate τ_i in the absence of τ, which are caused by preexisting (subscript p) dislocation pile-up of length l_p consisting of N_p dislocations. Then at $\tau=0$, Eq. (5) is valid with τ_i and l_p substituted for τ and l, and Eq. (10) can be transformed to

$$p=f(\theta)+\frac{\Gamma}{\varepsilon}\sqrt{\frac{\Gamma}{5k\theta n}}-0.25\tau_i l_p\sqrt{\frac{\Gamma}{5k\theta n}\left[1+\left(\frac{\gamma}{\varepsilon}\right)^2\right]}n\ln\frac{2}{n}. \quad (11)$$

The first term in Eq. (10) is designated as $f(\theta)$, where $p=f(\theta)$ represents the equation of the SC line for an infinitely long waiting time in the absence of τ, τ_i, and defects. If K

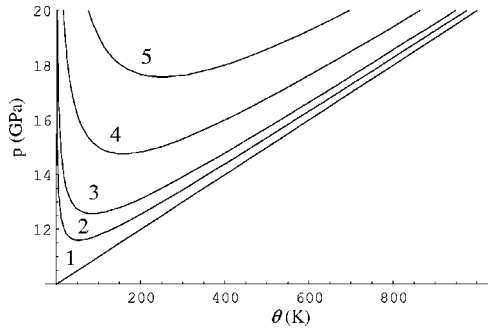

FIG. 6. Relationships of SC pressure vs temperature for thermally activated nucleation at dislocation pile-up for several values of $\tau_i l_p = \tau l$, expressed in 10^{-9} GPa m: 1, the equilibrium PT line; 2, $\tau_i l_p = 5.6$; 3, $\tau_i l_p = 5.2$; 4, $\tau_i l_p = 4.0$; 5, $\tau_i l_p = 2.0$.

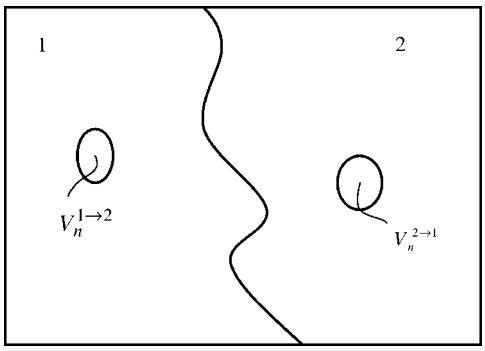

FIG. 7. Representative volume V consisting of a mixture of phases 1 and 2. $V_n^{1\to 2}$ and $V_n^{2\to 1}$ are small volumes of phase 1 and 2 undergoing SC.

and Eshelby energy is negligible, $f(\theta)$ represents an equilibrium line between phases. Since the term $\tau\gamma/\varepsilon$ in Eq. (10) is negligible, the effect of both τ and τ_i can be expressed in terms of the number of dislocations in pile-up [see Eq. (6)]. Let us start with the case when $N = N_p$ (i.e., $\tau l = \tau_i l_p$). Then Eqs. (10) and (11) give practically the same result. In Fig. 6, relationships $p(\theta)$ are plotted for the equilibrium PT line $p = f(\theta) = 10 + \theta/100$, and for lines described by Eq. (11) [or Eq. (10)] for several values of $\tau_i l_p = \tau l$. Deviation from the equilibrium line is a kinetic effect which decreases with temperature growth. Let, e.g., $\tau_i l_p = 5.2 \times 10^{-9}$ GPa m with no external stresses. Above some temperature, say $\theta \simeq 500$ K, deviation of Eq. (11) from the equilibrium line is within the experimental error, and the experimental kinetic curve can be used to determine the "equilibrium" phase diagram.

By applying an external stress, we do not change the local stresses τ_l and σ_l due to preexisting pile-up and the "equilibrium" phase diagram (as is observed in experiments[22]), if the number of dislocations N_p in pile-up does not change. Indeed, for given N_p, the local stresses are independent of applied stress (external plus internal), see Eqs. (5) and (6). However, an external stress produces new dislocation pile-ups. The difference between preexisting defects and defects with the same N nucleated during plastic flow is outlined in the following. After exhausting all preexisting defects, kinetics of pressure-induced PT is saturated. For strain-induced nucleation, many more defects can be generated and more product phase can appear. This was observed in experiments[22] for $PbO_2 I \to PbO_2 II$ PT: kinetics with shear is the same as without shear at the beginning of PT and much more intensive for a larger time. If $N > N_p$ ($\tau l > \tau_i l_p$, e.g., $\tau l = 5.6 \times 10^{-9}$ GPa m), in particular when new dislocations are generated in preexisting pile-ups, then external shear again does not change "phase equilibrium" conditions (Fig. 6), but reduces the temperature at which PT occurs at "phase equilibrium" conditions, as it occurs in experiments.[22] Consequently, experimental results[22] (item 1) can be explained by considering the thermally activated regime and taking into account preexisting defects of potency comparable with strain-induced defects.

Remark 1. Similar consideration can be done for pile-up of screw dislocations. However, they are less effective because they do not produce normal stresses and the shear stress is smaller by a factor of $1/(1-\nu)$ than for edge dislocations.

Remark 2. Gilman's mechanism[6] may be real in the region of high stress concentration and, consequently, large elastic shear. At the macroscale, elastic shear is limited by the yielding and does not exceed $\tau_y/(2\mu) = 10^{-3} - 10^{-2}$.

V. MICROSCALE TREATMENT

Let us summarize the results of nanoscale study which will be conceptually incorporated in the microscale model. We will consider barrierless strain-induced nucleation at strong defects which leads to the strain-controlled kinetics. Since the contribution of the stress concentration to the driving force for SC is finite, there exists a lowest possible pressure, p_ε^d, below which strain-induced SC is impossible. Defects generate both compressive and tensile pressure, which are of the same magnitude, e.g., for dislocation pile-ups. Consequently, they simultaneously promote both direct and reverse SC in different regions. Moreover, for two phase mixture 1+2, the stronger the phase 2 is, the smaller fraction of the plastic strain is concentrated in it. For CR, plastic flow produces a fragmentation and mixing of components similar to liquid phase CR,[8] so mixing will not be considered as the limiting factor. We believe that the above facts represent basic microscopic reasons for the mechanochemical phenomena considered in Sec. II.

Let us consider a representative volume V consisting of a mixture of material 1 and 2 which can transform to each other via SC (Fig. 7). Plastic deformation of the volume V will be described in terms of equivalent plastic strain q (Odqvist parameter,[35,36] $\dot{q} := (2/3\boldsymbol{d}_p : \boldsymbol{d}_p)^{1/2}$, $\boldsymbol{d}_p$ is the plastic strain rate) with values q_1 and q_2 in phases 1 and 2. Strain-induced SCs $1 \to 2$ in phase 1 and $2 \to 1$ in the phase 2 occur simultaneously. Our goal is to derive the strain-controlled kinetic equation $dc/dq = f(p,c)$, where c is the volume fraction of phase 2 and p is the macroscopic pressure applied to V. Since time is not an explicit parameter, a kinetic equation has to be derived using the thermodynamic criterion $F = 0$ and averaging procedure which is extremely complex. To obtain a simple analytical expression, we approximate the microscopic transformation work averaged over the transforming volume $V_n^{1\to 2}$ (Fig. 7) by decreasing the function of

dc/dq_1 [Eq. (13)]. The validity of such an approximation follows from our finite element modeling.[29] Resolving the thermodynamic SC condition for dc/dq_1 [Eq. (14)], we obtain the strain-controlled kinetic equation for SC $1\rightarrow 2$. Repeating the same procedure for SC $2\rightarrow 1$ and expressing q_1 and q_2 via q and the yield stresses σ_{y1} and σ_{y2} of phase 1 and 2 [Eq. (15)], we obtain the final expression (16) for $dc/dq = f(p,c)$. Analysis of the stationary solution of Eq. (16) [see Eq. (17)] allowed us to explain some experimental phenomena enumerated in Sec. II and suggest some methods to control SCs.

Let us make the following simplifications. We decompose stress, $\boldsymbol{T}$, into a sum of the macroscopic part $\boldsymbol{T}_m$, which is homogeneous in a representative volume $V \gg V_n$, and the microscopic contribution, $\tilde{\boldsymbol{T}}$, which fluctuates inside of the volumes V and V_n. As $V \gg V_n$, the variation of the macroscopic stress, $\boldsymbol{T}_m$, is negligible during a small SC increment. Maximum macroscopic shear stress, $\tau < \tau_y$, is smaller by a factor of 10-100 than the pressure in the center of the disk, see Sec. VI. It will be neglected. Because of the relatively large size of the transforming region, the surface energy is neglected as well. Then the thermodynamic SC criterion $F=0$,

$$X \coloneqq p\varepsilon_o + \frac{1}{V_n}\int_{V_n}\int_{\mathbf{0}}^{\boldsymbol{\varepsilon}_{t2}} \tilde{\boldsymbol{T}}:d\boldsymbol{\varepsilon}_t dV_n - \Delta\psi(\theta) = K, \qquad (12)$$

where $p=1/3\boldsymbol{I}:\boldsymbol{T}$ is the macroscopic hydrostatic pressure and ε_0 is the volumetric transformation strain. To calculate the integral in Eq. (12), the specific mechanism of strain-induced nucleation has to be known and then the corresponding boundary-value problem has to be solved numerically. For example, the nucleation at the shear-band intersection in TRIP steel was investigated in our paper[29] using the PT criterion Eq. (12) and a finite element method (FEM) solution of the corresponding problem. It was found that the transformation work decreases (almost linearly in Ref. 29) with the growth of $\Delta c/\Delta\varepsilon_p \simeq dc/d\varepsilon_p$, where $\Delta\varepsilon_p$ is the prescribed small, uniaxial averaged plastic strain increment. Qualitatively, this has to be the case for any mechanism of nucleation at strain-induced defects, e.g., at slip band and dislocation pile-up, considered above. However, to find explicit relations, additional statistical assumptions and bulky numerics are required. To approximately take into account, in an averaged over V microscopic SC criterion, the contribution of nano- and microscopic mechanisms of strain-induced nucleation, we substitute the integral with its approximate estimate

$$X_d \coloneqq p\varepsilon_o - \Delta\psi + \Delta X_d\left[1 - \frac{a}{(1-c)^{\zeta}}\left(\frac{dc}{dq_1}\right)^{\chi}\right] = K_d. \quad (13)$$

Here ΔX_d is the maximal microscopic contribution to transformation work (at infinitesimal dc/dq_1), and a, χ, and ζ are parameters. The factor $(1-c)^{\zeta}$ takes into account that SC $1\rightarrow 2$ occurs in phase 1 only. Let us define the SC equilibrium pressure p_e by the condition $p_e\varepsilon_o - \Delta\psi = 0$, the pressure p_h^d under which SC can occur under the hydrostatic condition without a strain-induced contribution by the equation $p_h^d\varepsilon_o - \Delta\psi = K_d$ (the energy of internal stresses is neglected for simplicity), and the minimal pressure p_{ε}^d under which SC can start by the equation $p_{\varepsilon}^d\varepsilon_o - \Delta\psi + \Delta X_d = K_d$. Then $\Delta X_d = (p_h^d - p_{\varepsilon}^d)\varepsilon_o$. Solving Eq. (13) for dc/dq_1, one obtains a thermodynamically consistent strain-controlled kinetic equation

$$\left(\frac{dc}{dq_1}\right)^{\chi} = \frac{(1-c)^{\zeta}}{a}\frac{p - p_{\varepsilon}^d}{p_h^d - p_{\varepsilon}^d}. \qquad (14)$$

If $p < p_{\varepsilon}^d$, then $dc/dq_1 = 0$. Simultaneously, strain-induced $2\rightarrow 1$ SC will occur in phase 2. It can be described by the following similar equations:

$$X_r \coloneqq p\varepsilon_o - \Delta\psi - \Delta X_r\left[1 - \frac{b}{c^k}\left(\frac{dc_1}{dq_2}\right)^m\right] = -K_r < 0;$$

$$\left(\frac{dc_1}{dq_2}\right)^m = \frac{c^k}{b}\frac{p_{\varepsilon}^r - p}{p_{\varepsilon}^r - p_h^r},$$

where $c_1 = 1 - c(c_2 = c)$, $\Delta X_r = (p_{\varepsilon}^r - p_h^r)\varepsilon_o > 0$ is the maximal microscopic contribution to transformation work at reverse SC, and k, b, and m are parameters; pressure p_h^r under which the reverse SC can occur under the hydrostatic condition without a strain-induced contribution is defined by the equation $p_h^r\varepsilon_o - \Delta\psi = -K_r$, and the maximal pressure p_{ε}^r under which the reverse SC can start is defined by the equation $p_{\varepsilon}^r\varepsilon_o - \Delta\psi - \Delta X_r = -K_r$. To define the Odqvist parameter for each phase, we assume $q_1/q_2 = (\sigma_{y2}/\sigma_{y1})^w$ and $q = c_1q_1 + c_2q_2$, where

$$q_1 = q\sigma_{y2}^w/\sigma_y;\ q_2 = q\sigma_{y1}^w/\sigma_y,\ \ \sigma_y \coloneqq c\sigma_{y1}^w + (1-c)\sigma_{y2}^w. \qquad (15)$$

According to Eq. (15), the stronger the phase is, the smaller fraction of the equivalent strain is concentrated in it; for $\sigma_{y1} = \sigma_{y2}$, one has $q_1 = q_2 = q$. As for $\sigma_{y2} = (4-10)\sigma_{y1}$, q_2 is negligible, we estimate parameter $w = (2-5)$. Adding algebraically rates of direct and reverse SC and taking into account Eq. (15), one obtains the final kinetic equation

$$\frac{dc}{dq} = \frac{\sigma_{y2}^w}{\sigma_y}\left(\frac{(1-c)^{\zeta}}{a}\right)^{1/\chi}\left(\frac{p - p_{\varepsilon}^d}{p_h^d - p_{\varepsilon}^d}\right)^{1/\chi} - \frac{\sigma_{y1}^w}{\sigma_y}\left(\frac{c^k}{b}\right)^{1/m}\left(\frac{p_{\varepsilon}^r - p}{p_{\varepsilon}^r - p_h^r}\right)^{1/m}. \qquad (16)$$

Equation (16) is valid for $p_{\varepsilon}^r > p_{\varepsilon}^d$, i.e., when both direct and reverse SCs occur simultaneously. If $p_{\varepsilon}^r < p_{\varepsilon}^d$, then one needs to keep the first term only for $p > p_{\varepsilon}^d$ and the second term only for $p < p_{\varepsilon}^r$; $dc/dq = 0$ for $p_{\varepsilon}^r < p < p_{\varepsilon}^d$. Stationary solution of Eq. (16) for the case $p_{\varepsilon}^r < p_{\varepsilon}^d$ is $c=1$ for $p > p_{\varepsilon}^d$; $c=0$ for $p < p_{\varepsilon}^r$; c is equal to its value before shear for $p_{\varepsilon}^r < p < p_{\varepsilon}^d$. For the case $p_{\varepsilon}^r > p_{\varepsilon}^d$ and $k/m = \zeta/\chi = g$, a stationary solution of Eq. (16) is found,

$$c_s = \frac{1}{1 + M(1-\tilde{p})^{1/k}/\tilde{p}^{1/\zeta}},\ \ \tilde{p} \coloneqq \frac{p - p_{\varepsilon}^d}{p_{\varepsilon}^r - p_{\varepsilon}^d}; \qquad (17)$$

$$M \coloneqq \left(\frac{\sigma_{y1}}{\sigma_{y2}}\right)^{w/g}\frac{a^{1/\zeta}}{b^{1/k}}\frac{(p_h^d - p_{\varepsilon}^d)^{1/\zeta}}{(p_{\varepsilon}^r - p_h^r)^{1/k}}(p_{\varepsilon}^r - p_{\varepsilon}^d)^{(1/k - 1/\zeta)}.$$

It follows from Eq. (17) that for $p \rightarrow p_{\varepsilon}^d$, one has $c_s = 0$. For $p \rightarrow p_{\varepsilon}^r$ (and for $p \geqslant p_{\varepsilon}^r$, i.e., when the reverse SC is impos-

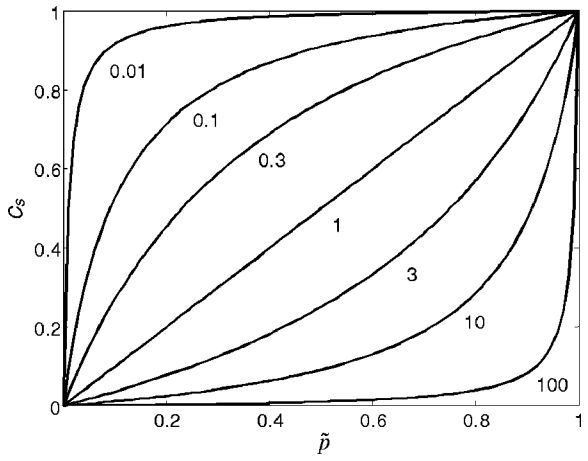

FIG. 8. Relation between the stationary value of the volume fraction of the second phase and dimensionless pressure. Numbers near curves designate values of M.

sible), one obtains $c_s=1$. Between these two pressures, c_s varies from 0 to 1 and the shape of the $c_s(p)$ curve depends on material parameters, see Fig. 8. In particular, if $M=1$ (e.g., for equal material parameters of both phases) and $\zeta=k=1$, then $c_s=\tilde{p}$. If $M\to 0$ (e.g., if the second phase is much stronger and/or $b^{1/k}/a^{1/\zeta}\to 0$, i.e., the kinetic of the reverse PT is suppressed), then $c_s\to 1$. In the opposite case, $M\to\infty$, $c_s\to 0$. If $c<c_s$, then direct SC will occur for straining under constant pressure $p_\varepsilon^r>p>p_\varepsilon^d$. In the opposite case, the reverse PT will take place. A number of conclusions can be made from our analysis.

1. If direct and reverse SC occur in the same pressure range (i.e., $p_\varepsilon^d\simeq p_h^r$ and $p_h^d\simeq p_\varepsilon^r$) and with comparable kinetics, then even if the pressure for the initiation of SC can be reduced significantly because of strain-induced nucleation, only a small amount of product phase can be produced at a small pressure around p_ε^d. A significant amount of product phase can be obtained under the pressure around p_h^d, i.e., like for pressure-induced SC.

A significant amount of high-pressure phase or complete SC can be induced by a large strain at low pressure if the kinetics of reverse SC is suppressed only, i.e., for a small M (Fig. 8). One of the conditions for a small M, $(\sigma_{y2}/\sigma_{y1})^{w/g}\gg 1$, shows that large plastic strains promote the appearance of hard phases more than weak phases. When this condition is fulfilled, then plastic flow localizes inside of phase 1 causing $1\to 2$ SC, while small plastic strain in phase 2 causes a small advance of the reverse SC.

2. Let us consider the case with $p_\varepsilon^d\neq p_h^r$ and $p_h^d\neq p_\varepsilon^r$. At $p_\varepsilon^d>p_h^r$, direct SC starts at a pressure which is larger than the reverse PT pressure at hydrostatic conditions, which is the case for most known PT. However, it is possible according to our estimates in Sec. IV A that $p_\varepsilon^d<p_h^r$, i.e., the direct PT starts at a pressure which is smaller than the reverse PT pressure at hydrostatic conditions. Such an unusual situation was observed for the PT semiconductor→metal in InSb, InTe, Ge, and Si.[15] This result was interpreted as a significant reduction in equilibrium PT pressure because of plastic shear. However, as was discussed above, p_ε^d can be lower than p_e, i.e., the above experimental results do not imply the change in p_e. The p_e does not appear in any equation for the strain-induced SC and consequently cannot be determined from strain-induced experiment.

3. Zero-pressure hysteresis was observed at pressure $p=1.8$ GPa for $B1\leftrightarrow B2$ PT in KCl,[16] and it was assumed that this is p_e. However, if the system is in a stationary state under any pressure p with $c=c_s$, then any infinitesimal pressure increase (decrease) followed by plastic straining will cause $1\to 2(2\to 1)$ SC, i.e., pressure hysteresis is zero.

4. Our analysis explains the contradictive statement in Sec. II that plastic straining reduces pressure hysteresis (item 3) and substitutes a reversible PT with irreversible ones (item 6), i.e., it increases the hysteresis. Hysteresis reduces when both direct and reverse SCs are strain-induced. Hysteresis increases when after large plastic strain, the reverse SC is not strain-induced (i.e., it is pressure-induced).

5. A matrix with a yield stress higher (lower) than that for reagents significantly promotes (suppresses) the CRs (Ref. 8 and item 10), because plastic strain is concentrated in the reacting material (matrix). Adding stronger particles to the material under study will facilitate SC and could cause SC which was not obtained otherwise, e.g., metallic hydrogen.[37] Adding weaker particles will suppress SC, which is important, e.g., for explosives.

6. The fact that the SC is promoted by plastic deformation at a pressure above p_ε^d only explains a seeming contradiction formulated in Ref. 9, namely why large plastic deformation during the compression of materials does not cause SC, while relatively small shear strain at relatively high pressure promotes SC significantly. Large plastic strain below p_ε^d suppresses SC because of strain hardening and growth of K_d.

The above results will be qualitatively the same for any reasonable kinetic equation, because they are based on experimental and theoretical facts that direct and reverse strain-induced SC can occur simultaneously, that there exist limiting pressures p_ε^d and p_ε^r, and that strain in the weaker phase is larger than in the stronger phase.

VI. MACROSCOPIC PLASTIC FLOW AND STRUCTURAL CHANGES

Stress, strain, and volume fraction c fields in a specimen compressed and sheared in RDAC are very complex and coupled. The kinetics of SCs is determined by pressure p and accumulated plastic strain q fields and, in turn, affects them. To analyze actual tests in RDAC, to be able to extract correct experimental information from them, to improve these tests, and to explain some phenomena enumerated in Sec. II, one needs to have a solution for the macroscopic plastic flow and SCs in a specimen. Without rotation of an anvil, FEM modeling was used to determine stress and strain fields without SCs.[38] For the case with the rotation of an anvil, the only known analytical solution is obtained in Ref. 9. The problem formulation in Ref. 9 is oversimplified; in particular, relative circumferential sliding of material with respect to the anvil is not properly taken into account. The properties of the solution with SC are analyzed qualitatively without giving the explicit solution, and only for the SC at the center of the specimen. In this paper, a much more detailed and precise

solution for plastic flow and SCs is found, which includes the definition of relative circumferential sliding. The strain-controlled kinetic equation for the SC derived in Sec. V is used. It was found that the *rotation of an anvil reduces the contact friction in the radial direction* and leads to the reduction of the specimen thickness under the fixed load. Macroscopic intensification of the SCs due to the rotation of the anvil is related to this thickness reduction, which *compensates a volume decrease due to SC and increases plastic strain, defect generation, and pressure*. When the yield stress of the product phase is larger (smaller) than the yield stress of the parent phase, *the pressure self-multiplication (self-demultiplication)* effect is derived. It is also found that the rotation of an anvil can lead to new phases, which not only were not, but also *could not be obtained without the rotation of the anvil*. The solution gives two possible explanations for the appearance of small "steps" at the pressure distribution near the diffuse interphase; one of them is related to the TRIP. Comparison is also made between SCs in RDAC and in traditional DAC. Some alternative methods to promote strain-induced SCs without the rotation of an anvil are suggested.

A. Problem formulation

Let us consider a problem of the compression of a thin cylindrical disk of current thickness h by an applied axial force P; at some thickness h_0, one anvil starts to rotate with angular velocity ω_a and rotates by angle φ_a under $P=\text{const}$ (Fig. 1). The axisymmetric problem formulation is adopted. The angular velocity of the deformed material ω differs from ω_a because of relative sliding. By putting the coordinate system $r\theta z$ in the moving gravity center of the disk, we will consider the rotation with velocity $\omega/2$ at $z=h/2$ and with $-\omega/2$ at $z=-h/2$. This will allow us to use a symmetry condition. We assume that the plastic deformations are large enough and the model of isotropic perfectly plastic material is applicable.[35] Some steps to the solution of this problem without SC (Refs. 9 and 39) are based on the assumption $\omega=0$. This contradicts experiments.[19] We will find the complete solution of this problem and generalize it to the case with SC. We will neglect the elastic deformations of the anvils and disk, pressure nonhomogeneity in the z direction, and use the simplified equilibrium equation,[35,39] as well as the continuity condition

$$\frac{\partial p}{\partial r} = -\frac{2\tau_r}{h}, \tag{18}$$

$$\frac{\dot{h}}{h} + \frac{\partial V_r}{\partial r} + \frac{V_r}{r} = -\varepsilon_0 \dot{c}(r). \tag{19}$$

Here r is the spatial radial coordinate, V_r is the radial velocity, and τ_r is the radial component of the shear frictional stress τ on the boundary S between the anvils and a disk. Boundary conditions are $p=\sigma_o+\sigma_y$ at the external radius of the anvil $r=R$, where σ_o is the pressure at $r=R$ due to the external support of the material being outside the working region of the anvils $r>R$; $V_r=0$ at $r=0$. Vector $\boldsymbol{\tau}$ is directed opposite to the velocity $\boldsymbol{v}_s=\{V_r;(\omega-\omega_a)r/2\}$ of relative sliding of a compressed material on the boundary S, where V_r and $(\omega-\omega_a)r/2$ are radial and circumferential components of $\boldsymbol{v}_s$ (Fig. 9). For a thin disk, $|\boldsymbol{\tau}|=\tau_y=\sigma_y/\sqrt{3}$ (von Mises yield condition is used), i.e., $\boldsymbol{\tau}=(\boldsymbol{v}_s/|\boldsymbol{v}_s|)(\sigma_y/\sqrt{3})$.

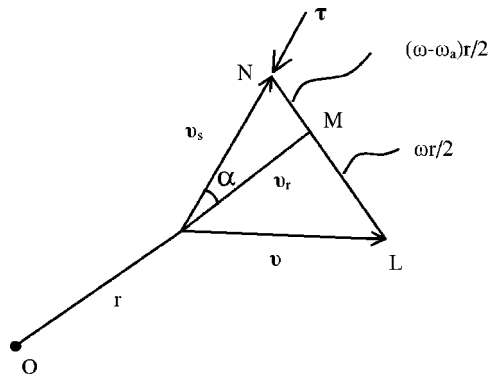

FIG. 9. Relative position of the material velocity $\boldsymbol{v}$ and velocity of relative sliding along the contact surface $\boldsymbol{v}_s$; $MN=(\omega-\omega_a)r/2$, $ML=\omega r/2$.

B. Solution for the case without structural changes

Velocity fields which satisfy Eq. (19) for $\dot{c}=0$ are

$$V_z = \frac{\dot{h}z}{h}, \quad V_r = -\frac{\dot{h}r}{2h}, \quad V_\theta = \frac{\omega r z}{h}. \tag{20}$$

The sliding velocity $\boldsymbol{v}_s$ and $\boldsymbol{\tau}$ are inclined at an angle α to the radius (Fig. 9) with

$$\cos\alpha = \{1+[(\omega-\omega_a)h/\dot{h}]^2\}^{-1/2}, \text{ thus } \tau_r = \sigma_y \cos\alpha/\sqrt{3}. \tag{21}$$

Integration of Eq. (18), taking into account Eq. (21), leads to (Fig. 10)

$$p = \sigma_o + \sigma_y[1 + 2(R-r)/\sqrt{3}H],$$

$$P = \pi R^2[\sigma_o + \sigma_y(1 + 2R/3\sqrt{3}H)], \tag{22}$$

$$H := h/\cos\alpha = h\sqrt{1+[(\omega-\omega_a)h/\dot{h}]^2} = h_0. \tag{23}$$

For compression without rotation, $\cos\alpha=1$ and $H=h$. For rotation at constant force, the equation $H=h_o$ follows from the conditions $P=\text{const}$ and $\sigma_o=\text{const}$. Equation (22) shows that at $P=\text{const}$ due to $H=\text{const}$, the pressure distribution is independent of rotation, which *corresponds to the experiments*.[16,20] Consequently, the rotation is equivalent to the *reduction* of *friction* in the radial direction and results in a *decrease* of the *disk thickness*. The greater the circumferential sliding along the anvil is, the greater the reduction in thickness is. The main task now is to find ω. We derived a simple equation (see Appendix A)

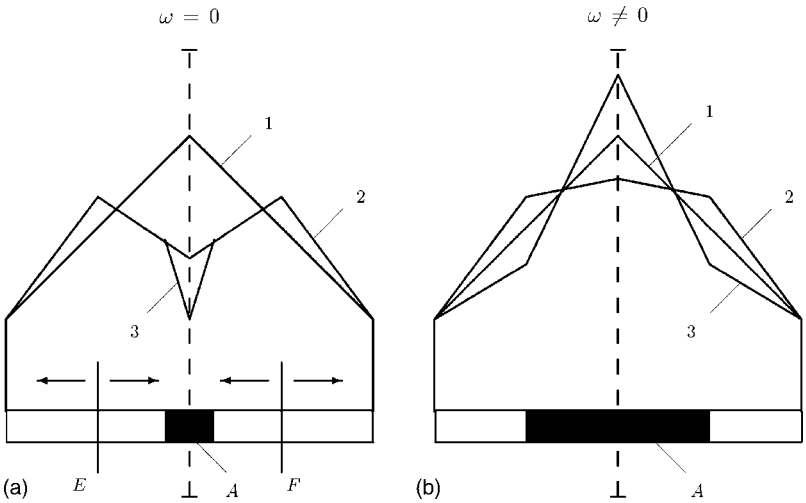

FIG. 10. Pressure distribution: (a) without rotation of an anvil: 1, before SC; 2, after SC at $\sigma_{y1}=\sigma_{y2}$; 3, after SC at $\sigma_{y1}<\sigma_{y2}$; (b) with rotation of an anvil: 1, $\sigma_{y1}=\sigma_{y2}$; 2, $\sigma_{y1}>\sigma_{y2}$; 3, $\sigma_{y1}<\sigma_{y2}$.

$$\omega-\omega_a=-\frac{0.204m}{1+0.204m}\omega_a,\quad m:=R/h_0, \tag{24}$$

which, surprisingly, is independent of $G:=h_0/h$. Substituting Eq. (24) in Eq. (23) results in the equation of reduction of thickness

$$d\bar{\varphi}:=\frac{0.204m}{1+0.204m}d\varphi_a=-\frac{dh}{h}\sqrt{\left(\frac{h_o}{h}\right)^2-1},$$

and

$$\bar{\varphi}=\sqrt{h_o^2/h^2-1}-\arccos(h/h_o). \tag{25}$$

Here $\bar{\varphi}$ is the angle of the relative sliding of an anvil with respect to the material. The plot of h/h_0 versus $\bar{\varphi}$ shown in Fig. 11 is in qualitative agreement with our experiments.[20]

The obtained results explain the seeming contradiction: *why does the rotation of the anvil reduce the PT pressure in the center of the disk where the plastic shear is absent?* The rotation induces a reduction in thickness and corresponding accumulated plastic strain $q=\ln(h/h_0)$, which induces the SC. The thickness reduction is remarkably large at small angles of twist (which agrees with experiments[20]); for $\bar{\varphi}\to 0$, $dh/d\bar{\varphi}\to\infty$. For small m, relative sliding and the reduction in thickness is smaller than at large m. At $m=5-10$, which is the smallest value for which our problem formulation is relevant and which is used in experiments, $\bar{\varphi}=(0.505-0.671)\varphi_a$. At $m\to\infty$, $\bar{\varphi}\to\varphi_a$, i.e., the torsion of the material is absent, but the reduction in thickness is the maximum possible. One of the conclusions is that the angle of material rotation rather than φ_a determines the parameter q in the kinetic equation and, consequently, has to be measured. At large m and φ_a, both the shear and compressive plastic strains are small, i.e., rotation at a fixed force is not effective for inducing the SC. Some ways to increase an effectiveness of the rotation are analyzed in Appendix B.

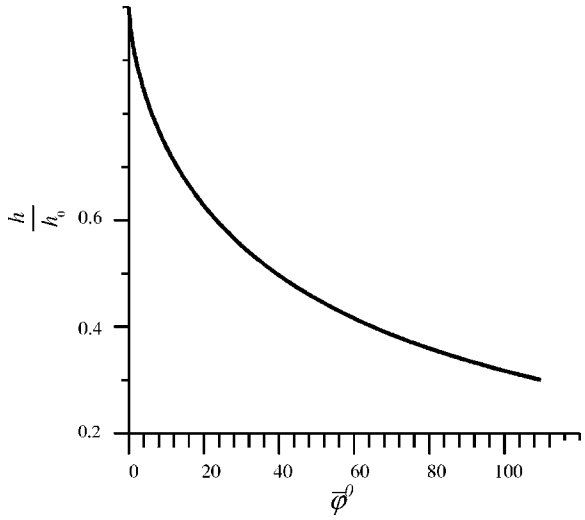

FIG. 11. Plot of relative thickness of specimen h/h_0 vs the angle of relative sliding of an anvil with respect to material $\bar{\varphi}$.

C. Analysis of structural changes

SC in the center of the disk: Interpretation of the measurements

Determine the pressure for the appearance of the first detectable amount, say $c_d=0.2$, of phase 2 in the center of the disk as a function of q. We neglect stress redistribution and the reverse SC. In the center $\hat{\gamma}=0$, $\dot{q}=-\dot{h}/h$, and $q=\ln(h_0/h)$. Equation (16) for small c can be simplified to

$$\frac{dc}{dq}=\frac{1}{a^{1/\chi}}\left(\frac{p-p_\varepsilon^d}{p_h^d-p_\varepsilon^d}\right)^{1/\chi}. \tag{26}$$

First, we determine the volume fraction c_0 of phase 2 during the compression (see Fig. 12) by integrating Eq. (26),

$$c_0=\frac{1}{a^{1/\chi}(p_h^d-p_\varepsilon^d)^{1/\chi}}\times\int_h^{h_1}\left[\sigma_y\left(1+\frac{2}{\sqrt{3}}\frac{R}{\hat{h}}\right)-p_\varepsilon^d\right]^{1/\chi}\frac{d\hat{h}}{\hat{h}}$$
$$\simeq\left(\frac{p_\varepsilon^d}{a(p_h^d-p_\varepsilon^d)}\right)^{1/\chi}\int_1^{\bar{p}}\frac{(p-1)^{1/\chi}dp}{p};\quad \bar{p}:=\frac{p}{p_\varepsilon^d}, \tag{27}$$

where Eq. (22) with $H=h$ and condition $p\gg\sigma_y$ were used. Here h_1 is the thickness corresponding to pressure p_ε^d. The relation between the fixed pressure and the strain q necessary for the appearance of the first detectable amount c_d of the

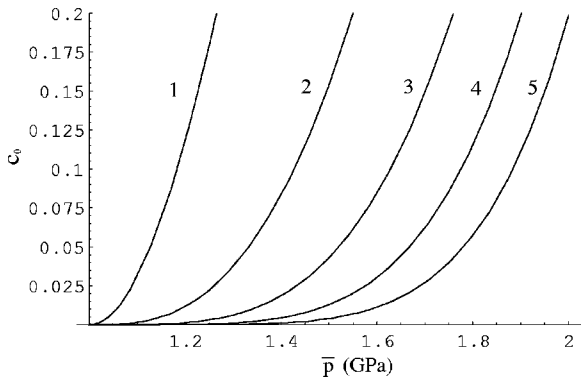

FIG. 12. Relationship between volume fraction of product phase obtained during compression c_0 and the pressure $\overline{p}$ for various values of χ. Numbers near curves designate values of $1/\chi$.

rotation of an anvil (see Fig. 13) can be found by integrating Eq. (26) at a fixed pressure,

$$\overline{p} = 1 + a\left(\frac{p_h^d}{p_\varepsilon^d} - 1\right)\left(\frac{c_d - c_0(p)}{\ln(h_0/h)}\right)^\chi. \tag{28}$$

We assume $p_\varepsilon^d = 1.25$ GPa, $p_h^d = 2.9$ GPa (i.e., $p_h^d/p_\varepsilon^d = 2.32$), $\varepsilon_0 = 0.11$, and $a = \varepsilon_0^\chi$, which is our approximate estimate for PT $B1 \to B2$ in KCl. Figures 12 and 13 allow us to explain, *why "plastic shear" significantly reduces the PT pressure in comparison with plastic compression*. Despite the fact that in both cases strain-induced PT in the center of the disk occurs under compression without shear, the *trajectories of the loading in the $\overline{p}$-q plane are very different*. This results in a different characterization of PT in terms of pressure. Under compression, pressure grows fast during the deformation process. That is why a detectable amount $c_d = 0.2$ can be obtained under a relatively high pressure only, e.g., at $p = 2.375$ GPa for $\chi = 0.25$. If, e.g., compression stops at $p = 1.825$ GPa, when $c_0 = 0.009$, then $c_d = 0.2$ can be reached after a rotation of an anvil resulting in $q = 1.47$. Traditionally, these results will be interpreted that PT pressure under hydrostatic conditions is 2.9 GPa, for the nonhydrostatic condition it is 2.375 GPa, and under large plastic shear it is

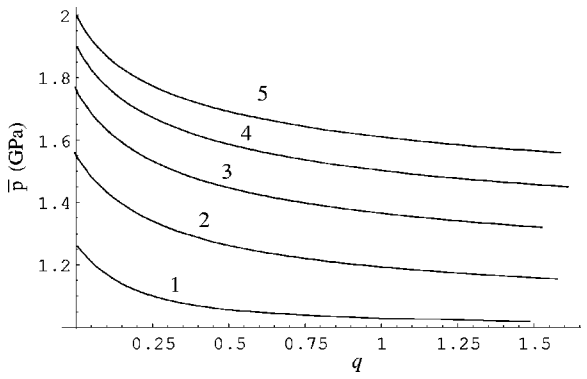

FIG. 13. Relationship between fixed pressure $\overline{p}$ and the strain q necessary for the appearance of the first detectable amount $c_d = 0.2$ of phase 2 in the center of a disk during rotation of an anvil. Numbers near curves designate values of $1/\chi$.

1.825 GPa. Now we understand that the numbers 2.375 GPa and 1.825 GPa do not characterize the "PT pressures," because they depend significantly on the loading path in the $\overline{p}$-q plane.

Kinematics

For the total strain rate, we put

$$e_z = -\frac{\dot{h}}{h},\ e_\theta = -\frac{V_r}{r},$$

$$e_r = \frac{\dot{h}}{h} + \frac{V_r}{r} + \varepsilon_0\dot{c},\ \hat{\gamma} = \frac{\partial V_\theta}{\partial z} = \frac{\omega r}{h}. \tag{29}$$

Let the transformation strain tensor consist of three equal, normal strains $1/3\varepsilon_0$ and transformation shear γ_t in the direction of torsion. The plastic strain rate is the difference between the total strain rate and the transformation strain rate,

$$e_z^p = -\frac{\dot{h}}{h} - 1/3\varepsilon_0\dot{c},\ e_\theta^p = -\frac{V_r}{r} - 1/3\varepsilon_0\dot{c},$$

$$e_r^p = \frac{\dot{h}}{h} + \frac{V_r}{r} + 2/3\varepsilon_0\dot{c},\ \hat{\gamma}^p = \frac{\omega r}{h} - \gamma_t\dot{c}. \tag{30}$$

Let $\dot{c} \neq 0$ in the ring $r_2 \leqslant r \leqslant r_1$, i.e., in the region $0 \leqslant r \leqslant r_2$, the SC into phase 2 is completed (in particular, $r_2 = 0$), and in the region $r \geqslant r_1$, the SC did not start yet. The continuity condition (19) can be satisfied by the following field:

$$V_r = -\frac{\dot{h}r}{2h} - \frac{\varepsilon_0\langle\dot{c}\rangle N r}{2} \quad \text{for } r_2 \leqslant r \leqslant r_1, \tag{31}$$

$$V_r = -\frac{\dot{h}r}{2h} \quad \text{for } r \leqslant r_2,$$

$$V_r = -\frac{\dot{h}r}{2h} - \frac{\varepsilon_0\langle\dot{c}\rangle(r_1^2 - r_2^2)}{2r_1} \quad \text{for } r \geqslant r_1, \tag{32}$$

where $\langle\dot{c}\rangle := 2\int_{r_2}^{r}\dot{c}\rho d\rho/(r^2 - r_2^2)$ is the mean volume fraction rate in the ring $r_2 \leqslant \rho \leqslant r$, and $N = 1 - (r_2/r)^2$. In Eq. (32), $\langle\dot{c}\rangle$ is calculated for $r = r_1$. Then in the ring $r_2 \leqslant r \leqslant r_1$,

$$e_\theta = \frac{\dot{h}}{2h} + \frac{\varepsilon_0\langle\dot{c}\rangle N}{2},$$

$$e_r = \frac{\dot{h}}{2h} - \frac{\varepsilon_0\langle\dot{c}\rangle N}{2} + \varepsilon_0\dot{c},$$

$$e_\theta^p = \frac{\dot{h}}{2h} + \frac{\varepsilon_0\langle\dot{c}\rangle N}{2} - \frac{1}{3}\varepsilon_0\dot{c},$$

$$e_r^p = \frac{\dot{h}}{2h} - \frac{\varepsilon_0\langle\dot{c}\rangle N}{2} + \frac{2}{3}\varepsilon_0\dot{c}. \tag{33}$$

SC and pressure distribution in the central part of the disk

Let us analyze qualitatively the pressure redistribution during the SC in the central part of the disk (Fig. 10) and its effect on SC. For $r_2=0$, Eqs. (31) and (32) simplify to

$$V_r = -(\dot{h}/h + \varepsilon_0\langle\dot{c}\rangle)r/2 \quad \text{for} \quad r \leqslant r_1,$$

$$V_r = -1/2(\dot{h}r/h + \varepsilon_0\langle\dot{c}\rangle r_1) \quad \text{for} \quad r \geqslant r_1. \tag{34}$$

During intensive SC in compression without rotation under the prescribed load P increment, thickness reduction can be relatively small ($-\dot{h}/h < \varepsilon_0\langle\dot{c}\rangle$) and some internal part of the disk material may move to the center of the anvil due to a volume decrease. This is also observed *experimentally*.[19] The radius of the neutral circle EF $r_n = -r_1 h\varepsilon_0\langle\dot{c}\rangle/\dot{h}$ is found from the condition $V_r=0$. Equation (18) is valid, but the shear stress in the region EF changes sign and in the region A the yield stress of the two-phase mixture σ_y, which depends on c, should be used. In the simplest case, $\sigma_y=(1-c)\sigma_{y1}+c\sigma_{y2}$. We also assume that the pressure is continuous across the interface. Then

$$p_1(r) = \sigma_0 + \sigma_{y1}[1 + 2(R-r)/\sqrt{3}h]$$

$$\text{for} \quad r_n \leqslant r \leqslant R,$$

$$p_{1n}(r) = p_1(r_n) - 2\sigma_{y1}(r_n - r)/\sqrt{3}h$$

$$\text{for} \quad r_1 \leqslant r \leqslant r_n,$$

$$p_2(r) = p_{1n}(r_1) - 2\sigma_y(r_1 - r)/\sqrt{3}h$$

$$\text{for} \quad r \leqslant r_1, \tag{35}$$

see Fig. 10(a). It is important to note that without rotation, the pressure in the transforming region decreases significantly, which suppresses the SC. The higher σ_{y2} is, the larger the pressure reduction in the transforming region is. The rotation of an anvil significantly reduces the thickness h and compensates the volume decrease due to SC, i.e., $-\dot{h}/h \geqslant \varepsilon_0\langle\dot{c}\rangle$. In this case, material flows from the center of the disk, shear stress does not change the sign, and pressure grows monotonically with the decreasing radius [Fig. 10(b)],

$$p_1(r) = \sigma_0 + \sigma_{y1}[1 + 2(R-r)/\sqrt{3}H]$$

$$\text{for} \quad r_1 \leqslant r \leqslant R,$$

$$p_2(r) = p_1(r_1) + 2\sigma_y(r_1 - r)/\sqrt{3}H$$

$$\text{for} \quad r \leqslant r_1. \tag{36}$$

Consequently, because of specific plastic flow, *pressure in the transforming region for the case with rotation of an anvil is greater than without rotation*. In addition, *rotation increases accumulated plastic strain*. This is one of the macroscopic reasons why the rotation of an anvil promotes SCs. According to Eq. (36), if the yield stress of the product phase $\sigma_{y2} > \sigma_{y1}$, the pressure increases in the transforming region [Fig. 10(b)], despite the volume decrease due to SC. This agrees with experiments exhibiting the effect of *pressure self-multiplication*.[16,20] In the opposite case, pressure decreases during the SC [Fig. 10(b)], which is also observed in experiments for PT from the semiconductor to the metal (weaker) phase in Ge under shear.[15,18] Further, if two alternative phases can appear as a result of SC which differ by σ_y only, then the material with the smaller σ_y appears in the case without rotation (as pressure is higher at $\sigma_{y1} > \sigma_{y2}$), and the *stronger phase will be obtained under compression with rotation* (as pressure is higher at $\sigma_{y2} > \sigma_{y1}$). This is one of the macroscopic reasons why the rotation of an anvil leads to phases, especially to strong phases, which *were not obtained under compression without rotation* (item 5).

By calculating force for the pressure distribution, Eq. (36), and making it equal to the force at the beginning of rotation, one finds

$$H = h_0\left[1 + \left(\frac{r_1}{R}\right)^3\left(\frac{\sigma_y}{\sigma_{y1}} - 1\right)\right].$$

Even for $\sigma_y/\sigma_{y1}=5$, if we limit ourselves to $r_1/R \leqslant 1/4$, we can use $H=h_0$ with an error not exceeding 6.25%, as well as all Eqs. (23)–(25). For an approximate estimate of the maximum possible transformation rate, we assume that a volume decrease due to SC is completely compensated by (or infinitesimally smaller than) the reduction of h. In this case, when infinitesimal radial flow from the disk center occurs, shear stress does not change the sign, and the pressure grows monotonically with a decreasing radius. The condition $V_r=0$ and Eq. (A5) result in

$$\dot{c}\varepsilon_o = -\dot{h}/h = \dot{\bar{\varphi}}(G^2 - 1)^{-0.5}. \tag{37}$$

Phenomena related to the nonconcavity of the yield surface

Note that the pressure distribution for PT $B1 \rightarrow B2$ in KCl without rotation of the anvil looks like in Fig. 10(b) rather than in Fig. 10(a), but with a much smaller (near zero) pressure gradient in the transforming region.[16,20] This means that the condition $-\dot{h}/h \geqslant \varepsilon_0\langle\dot{c}\rangle$ is fulfilled for the case without rotation of the anvil and material does not flow to the center of the disk. Because $\sigma_{y2} > \sigma_{y1}$, the *pressure gradient grows significantly during PT under rotation and it is not clear why it reduces during PT without rotation of the anvil*. One of the possible reasons for this phenomenon can be related to the *transition from the plastic to elastic state under axial compression* in Bridgman anvils.[35] Namely, after the plastic compression of the thin disk, beginning with some value of force (thickness), an elastic region arises at the center of the disk and expands during further increase in applied force. This means that even an arbitrary large force cannot reduce the residual thickness of the disk below some critical value. One of the possible reasons suggested in Ref. 35 is related the to concave yield surface of the compressed material along the hydrostatic axis. This means that $d\sigma_y/dp$ is the growing function of pressure. Such a pressure dependence of the yield stress was observed in numerous experiments summarized in Refs. 13 and 35.

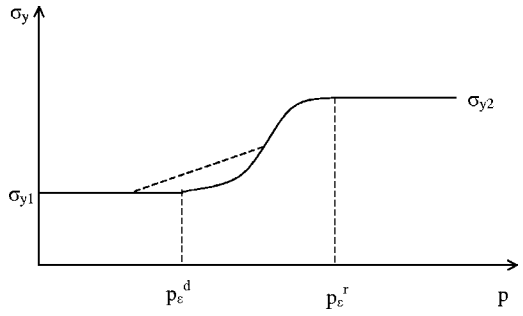

FIG. 14. Example of the concave yield surface (curve) when a high-pressure phase has greater yield stress than a low-pressure phase.

The existence of a solution of the problem of plastic limit equilibrium can be proved for the nonconcave yield surface only.[36] Therefore, one can expect that for a concave yield surface, the solution may not exist, and in fact the *disk cannot be compressed plastically*. In Ref. 35, an example of impossibility to continue a slip line field from the edges of the disk to its center was demonstrated for a concave yield surface. It is related to the strong growth of the yield stress and the friction stress from the edges of the disk to its center.

One of the reasons for the growth of $d\sigma_y/dp$ with the pressure growth can be related to SC from a weaker to a stronger phase which is spread over some pressure range. If, e.g., $\sigma_y=(1-c)\sigma_{y1}+c\sigma_{y2}$, then according to the stationary solution Eq. (17), the yield stress is pressure-independent for pressures corresponding to pure parent and product phase and grows with pressure between p_ε^d and p_ε^r (Fig. 14). Because there are straight lines connecting two points of the function $\sigma_y(p)$ which are located above the plot of $\sigma_y(p)$, the yield surface is concave and all arguments presented in Ref. 35 are valid. Consequently, after some progress of SC in the center of the disk, elastic deformation rather than plastic deformation takes place there. Then the friction shear stress is significantly smaller than σ_y and the pressure gradient is much smaller as well. Also pressure-induced SCs (which are less intensive) rather than strain-induced SCs can occur in the elastically deformed region which require $p \geqslant p_h^d$. Under the rotation of an anvil, shear stress in a radial direction decreases significantly [see Eq. (21)] so the boundary conditions are less critical for the nonexistence of a plastic solution discussed in Ref. 35. That is why plastic flow and strain-induced SCs occur during the rotation of an anvil. The greater σ_y, the greater the difference between compression and compression with rotation.

Let two alternative phases which differ by σ_y only appear as a result of SC, and the material with the smaller σ_y appear under compression without rotation. Material does not flow to the center of the disk with and without rotation. The rotation can promote the appearance and growth of the high-strength phase, because *rotation transforms stress-induced SC to strain-induced SC*, and causes significant pressure growth due to the *pressure self-multiplication effect* during the SC. This is an additional argument why the rotation of an anvil is the perspective way to *search for new superhard materials*.

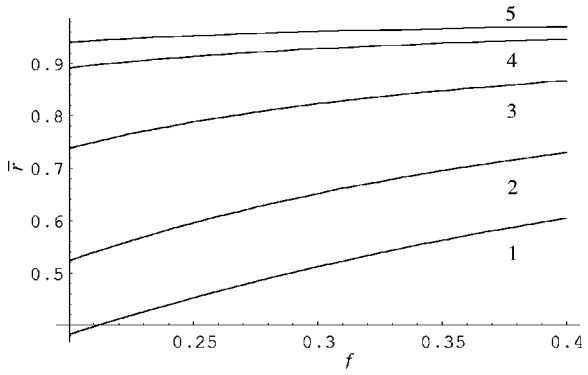

FIG. 15. Relationship $\bar{r}:=r_2/r$ vs $f:=r/R$ obtained from the condition $\dot{c}\varepsilon_o/\dot{q}=1$ for several values of $G:=h_0/h$: 1, $G=1.3$; 2, $G=1.5$; 3, $G=2$; 4, $G=3$; 5, $G=4$.

Possible reasons for "steps" on the pressure distribution

A small region with almost constant (sometimes even decreasing) pressure (Fig. 2) corresponds to a two-phase mixture where SC occurs (item 2). We will try to find possible explanations of this anomaly in pressure distributions. As follows from Eq. (18), τ_r has to be very small. This is possible, in particular, when for some r in the ring $r_2 \leqslant r \leqslant r_1$ one has $V_r=0$ in Eq. (31) and

$$\langle \dot{c} \rangle = -\dot{h}/(h\varepsilon_0 N). \tag{38}$$

The region near the neutral circle with $V_r=0$ is the stagnation region, where relative sliding with respect to the anvil is small and the shear stress grows slowly from zero at the neutral circle. If $\langle \dot{c} \rangle$ in Eq. (38) is not larger than the maximum transformation rate in Eq. (37), then the condition $V_r=0$ is plausible. The value of $\langle \dot{c} \rangle$ according to Eq. (38) is larger than in Eq. (37) for the same $\dot{h}/h$ [since $N=1-(r_2/r)^2<1$], however because of shear strain, $-\dot{h}/h$ in Eq. (38) represents only part of $\dot{q}$. We will calculate $\dot{q}$ to be used in the kinetic Eq. (16) based on a solution without SCs, i.e., on Eqs. (24), (A3), and (A5),

$$\omega = -\frac{\dot{h}}{0.204mh}\sqrt{G^2-1},$$

$$\dot{q} = \frac{1}{h}\sqrt{\dot{h}^2+\omega^2 r^2/3} = \frac{\dot{h}}{h}\sqrt{1+8(G^2-1)(r/hm)^2}. \tag{39}$$

Let us express $\dot{h}/h$ from Eq. (39) and substitute it in Eq. (38). We estimate whether parameter

$$\langle \dot{c} \rangle \varepsilon_o/\dot{q} = [N\sqrt{1+8(G^2-1)(Gr/R)^2}]^{-1} \tag{40}$$

can be equal to 1, like in Eq. (37). In Fig. 15, the relationship $\bar{r}:=r_2/r$ versus $f=r/R$ obtained from the condition $\dot{c}\varepsilon_o/\dot{q}=1$ is plotted for several values of G. In experiments, the minimal reasonable value r_2/r exceeds 0.8. This value can be exceeded for $G>2$ and $f>0.3$ or for $G>3$ for any f, which is realistic for some cases. However, this condition cannot be fulfilled for small $G<1.3$ and $f<0.2$, when steps still can be observed experimentally. Consequently, the condition $V_r=0$

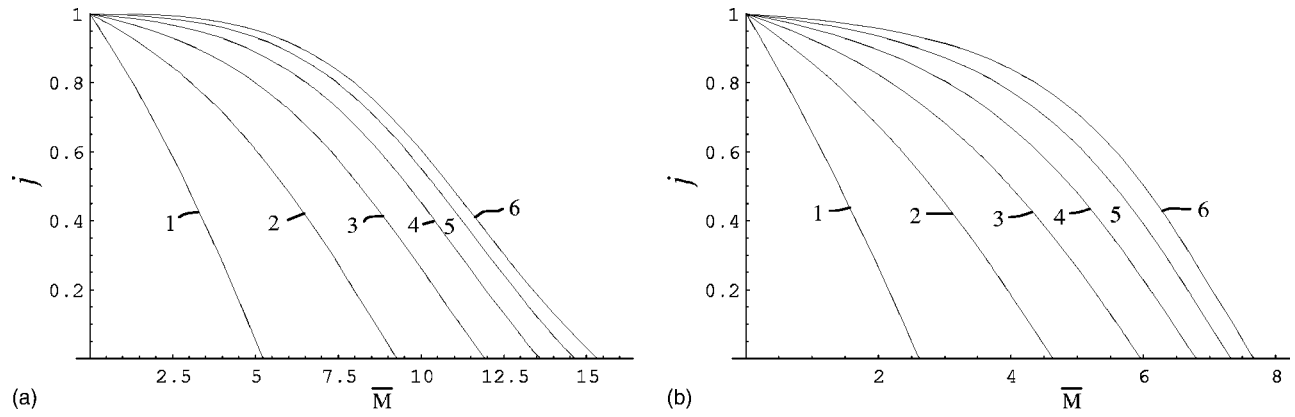

FIG. 16. Plots $j := \tau/\tau_0$ vs $\bar{M}$ for several values of $u := r/h$: (a) $\gamma_t = 0.1$; (b) $\gamma_t = 0.2$. Numbers near the curves designate values of u.

can be the reason for steps on a pressure distribution for a relatively large G and f, and it cannot be the reason for a small G and f.

As an alternative (or additional) reason for steps on a pressure distribution, we will consider the reduction of shear stresses under a prescribed shear strain due to TRIP (Refs. 27 and 40) or RIP.[3] The main idea of these phenomena is that the transformation strain produces huge internal stresses, which in combination with external stresses (which can be significantly smaller than the yield stress) cause plastic flow. The total plastic deformation rate consists of contributions due to traditional plasticity, which depends on stress, and due to TRIP (RIP), which is $\sim \dot{c}$, see Eqs. (30) and (33). In Refs. 3, 9, and 12, where analytical solutions for the problem on SCs in a thin layer (e.g., surface layer or shear band) were derived, the explicit expression between τ, plastic shear strain due to TRIP (RIP), γ, and $\boldsymbol{\varepsilon}_0$ was obtained. One of the results was that when $\tau \to \tau_y$, $\gamma \to \infty$. Consequently, for any finite prescribed γ, $\tau < \tau_y$. That is why TRIP is considered as a mechanism of shear (deviatoric) stress relaxation. We expect (because during rotation the shear strain increment $\Delta\varphi_a r/h$ is prescribed) the shear stress at the contact surface will relax significantly due to TRIP (RIP). A similar situation may happen during compression without rotation. However, because our model operates with strains averaged over the thickness, shear strain γ_{rz} disappears from consideration. We will estimate now shear stress in the direction of rotation $\tau = \tau_{z\theta}$ and assuming $\tau_r = \mathrm{cotan}\alpha\tau_{z\theta}$ with the same α as for the regions without SC [see Eq. (21)], and we will find how τ_r reduces due to TRIP (RIP). Consequently, it is sufficient to estimate τ/τ_0, where τ_0 is determined for the deformation without SC. Using Eq. (A3) for the dissipation rate, $D := \sigma_y \dot{q} = \sigma_y \sqrt{2/3}\sqrt{e_z^{p2} + e_r^{p2} + e_\theta^{p2} + 2(\hat{\gamma}^p/2)^2}$, one obtains according to the associated flow rule[35,36]

$$\tau = \frac{\partial D}{\partial \hat{\gamma}^p} = \sigma_y \frac{\partial \dot{q}}{\partial \hat{\gamma}^p} = \frac{\sigma_y}{\sqrt{6}} \frac{\hat{\gamma}^p}{\dot{q}}. \tag{41}$$

To calculate $\dot{q}$, we assume $\langle \dot{c} \rangle = \dot{c}$. Then, substituting Eqs. (30) and (33) in Eq. (41), one obtains

$$\tau = \sigma_y \frac{\omega r - \gamma_t h \dot{c}}{\sqrt{\dot{c}^2\{\varepsilon_0^2[4 + 3N(N-2)] + 3\gamma_t^2\}h^2 + 6h\dot{c}(\varepsilon_0 \dot{h} - \gamma_t \omega r) + 3(3\dot{h}^2 + \omega^2 r^2)}}. \tag{42}$$

Now we express $\dot{h}$ from Eq. $(39)_1$, $\dot{h} = Ch\omega$, $C := -0.204m/\sqrt{G^2 - 1}$, express $\dot{c} = \bar{M}\dot{q}$ with $\bar{M}$ determined from kinetic Eq. (16), and use Eq. $(39)_2$ for $\dot{q}$. After the substitution of all of these results and $u = r/h$ in Eq. (42), we arrive at the following equation:

$$\tau = \sigma_y \frac{u - \bar{M}\gamma_t \bar{C}}{\sqrt{\{\varepsilon_0^2[4 + 3N(N-2)] + 3\gamma_t^2\}\bar{C}^2\bar{M}^2 + 6\bar{C}\bar{M}(\varepsilon_0 C - u\gamma_t) + 9\bar{C}^2}}, \tag{43}$$

$\bar{C} := \sqrt{u^2/3 + C^2}$. Putting $\bar{M} = 0$ in Eq. (43), we obtain $\tau_0 = \sigma_y u/(3\bar{C})$. Plots $j := \tau/\tau_0$ versus $\bar{M}$ for several values u and $\gamma_t = 0.1$ and $\gamma_t = 0.2$ are presented in Fig. 16. Other parameters are $\varepsilon_0 = 0.1$, $m = 10$, and $G = 1.5$ (i.e., $C = -1.82$). The results are weakly dependent on N for $0 \leqslant N \leqslant 0.36$, which is why we used the fixed value of $N = 0.19$. For both γ_t, parameter j reduces significantly with the growth of the parameter $\bar{M}$ which characterizes the intensity of SC kinetics. The closer the SC region is to the center of the disk, the more intensively the shear stress reduces. Note that the estimated

maximum value of $\bar{M}$ determined from Eq. (37) is $\bar{M}=1/\varepsilon_0=10$. For $\gamma_t=0.2$ and for all $u\leqslant 6$, $\tau=0$, i.e., friction and consequently the pressure gradient are absent. For $\gamma_t=0.1$, the same is valid for $u\leqslant 2$. We did not continue plots for a negative j, because for polycrystalline material for a small τ, the transformation shear γ_t is not a constant. It reduces with the reduction of τ and is zero for $\tau=0$.

We can conclude that the *relaxation of shear friction stresses due to TRIP (RIP) can be partially or completely responsible for the appearance of small steps with almost constant pressure in the transforming zone*.

Remark 3. To integrate kinetic Eq. (37), one has to follow the material rather than the spatial points. This means that the Lagrangian rather than the Eulerian description has to be used. Even when $\sigma_{y1}=\sigma_{y2}$ and the pressure distribution is independent of rotation, the pressure in the material particles reduces because of radial flow. For some material particles after direct SC, this can cause the reverse SC. Probably, this is the case in (or near) the regions where "steps" on pressure distributions are observed.

Alternative methods to promote structural changes

The main macroscopic reasons for the promotion of SCs due to the rotation of the anvil is related to the possibility of additional axial displacement, which compensates a volume decrease, and increases p, q, and defect generation. Based on this understanding, we can suggest some alternative ways to obtain additional displacement without rotation.

(a) One possibility is to decrease σ_y and σ_0 at a constant external force, e.g., due to the heating of the external part of the disk or of the whole disk. By making equal the force before and during heating, one finds an explicit expression for h versus temperature rise. The modification of all the equations of Sec. VI C for this case is straightforward. As in the case with the RDAC, if a new phase is harder, the pressure increases in the center of the disk, see experiments in Ref. 41. Note that if the temperature is higher than the annealing temperature, then defect annihilation occurs, which eliminates strain hardening and leads to an additional reduction of the yield stress by a factor of 2–3 and higher.[35] Also, the effect of temperature on $\Delta\psi$ and on nanoscale mechanisms has to be taken into account.

(b) The other possibility may be based on the use of TRIP (RIP). Let us consider a two-phase material consisting of inclusions in a matrix. If under cyclic temperature variation inclusions undergo the cyclic direct-reverse PT with large enough ε_0, then the matrix will be deformed plastically, even without external stresses. External stress produces plastic strain in the direction of its action, which is proportional to the value of the applied stress and the number of thermal cycles (see experiments in Ref. 40 and our FEM modeling in Ref. 28). If we introduce the transforming particles into the disk compressed in the anvils, then it is possible to use the thermal cycles instead of the rotation of an anvil to get additional displacement and to promote the SC in the center of the disk.

(c) The most impressive way to reduce a disk thickness, based on rotational plastic instability, which resulted in the reduction of the pressure for the initiation of martensitic PT rBN to diamondlike cBN by one order of the magnitude, is described in Ref. 10.

VII. POSSIBLE EXPERIMENTAL CHARACTERIZATION OF STRAIN-INDUCED STRUCTURAL CHANGES UNDER HIGH PRESSURE

It is clear that pressure alone is not sufficient for the characterization of SC under nonhydrostatic conditions and plastic straining because it strongly depends on τ and q. Even for hydrostatic conditions, the pressure hysteresis is quite high for materials with large $\boldsymbol{\varepsilon}_0$. This does not allow experimental determination of p_e, and also reduces its significance. Equilibrium pressure can be determined theoretically using thermodynamic data or atomistic calculations, but the actual direct (reverse) SC occurs under much higher (lower) pressure. Because shear straining in the RDAC reduces PT hysteresis (item 3), it was claimed that plastic shearing allows us to better localize p_e. However, in some cases, direct PT pressure under shear is lower than p_e (item 4). As was demonstrated in Secs. IV and V, the p_e does not appear in any equation for the strain-induced SC and consequently cannot be determined from strain-induced experiment. SCs occurring in RDAC and in nonrotational DAC during plastic compression are strain-induced SCs under high pressure rather than pressure-induced SCs. This is not a terminology problem; it defines mechanism and a way to describe the SCs. In contrast to pressure-induced SCs, which predominantly occur at preexisting defects, strain-induced SCs occur at new defects generated during plastic flow. Based on the results of Sec. V, strain-induced SCs under high pressure can be characterized by a strain-controlled kinetic equation of the type

$$dc/dq = f(p,q,\theta,c,\sigma_{y1},\sigma_{y2}) = f_1(p,q,\theta,c), \qquad (44)$$

where σ_{yi} were excluded as functions of p, q, and θ. Kinetic Eq. (16) is an example of such a relationship. In the first approximation, the stress deviator (or shear stress) is not an explicit argument of Eq. (44), because its components are small in comparison with pressure. Also, its magnitude is equal to σ_y, so its effect is included implicitly. Such a characterization is consistent with characterization and modeling of strain-induced PTs in TRIP steels under normal pressure.[27] There is a basic difference between traditional time-dependent kinetics and strain-controlled kinetics. For time-dependent kinetics, for infinitesimal dc/dt and long enough experiments, it is possible in some cases to determine p_e. Kinetic description, which depends upon many parameters, is an addition to the phase equilibrium diagram, which depends on thermodynamic parameters only. In contrast, *strain-controlled kinetics is derived from the thermodynamic condition $F=0$ with proper allowance for all dissipative forces. Because p_e does not characterize strain-induced SCs at all, a strain-controlled kinetic equation is not additional, but the only way to characterize strain-induced SCs.*

Possible experimental ways to determine the kinetic equation

To determine experimentally all parameters in Eq. (44), one has to determine experimentally or to calculate a small increment Δc corresponding to a small increment Δq and the

current values of p, q, c, and θ locally in some small volumes. If the distributions of all of these fields can be determined, one can determine function f_1 (or f) from the few experiments. The pressure distribution can be measured using a ruby fluorescence technique (Fig. 2), x-ray diffraction with synchrotron radiation (when equations of state of materials under study or sensor-material are known), or Raman spectroscopy (after preliminary calibration). Displacement distribution at the contact surface between the sample and anvil can be measured by the imaging of ruby particle positions.[19] For the measurement of the thickness of the compressed disk under load, the method based on the electric capacity sensor can be used.[20] To increase the accuracy of this method, the elastic deformation of anvils and the support structure have to be taken into account using FEM.[38] As a result, the entire profile of the specimen under the load can be obtained. An alternative method for the measurement of the entire profile of the specimen is based on the measurement of the x-ray absorption.[42] When the displacement increment field during time Δt, the thickness, and thickness increment are known, one can approximately determine deformation rate fields [using definitions in Eq. (A1)] and calculate $\dot{q}$ [using Eq. (A3)]. For the measurement of the phase distribution, x-ray diffraction with synchrotron radiation, Raman spectroscopy, or Fourier transform infrared spectroscopy can be used. Note that one has to relate all parameters to the same material rather than spatial particles. That is why it is reasonable to "personalize" ruby particles and relate all measurements to the neighborhood of each (or some) particles. The above procedure can be used to check the validity and generalize or specify the kinetic Eq. (16). In addition to the complete characterization in terms of the kinetic equation, partial characterization by the parameters p_ε^d and p_ε^r, function $c_s(p)$, and plots of the relationship between the fixed pressure and accumulated strain q, which is necessary for the appearance of several prescribed fractions c_i of phase 2 (both for direct and reverse SC), is very useful.[15]

Remark 4. At the nanoscale, a condition of the type of Eq. (9), i.e., $p=\hat{f}(\tau,l,L,n,\theta)$, in principle can be used for the experimental characterization of strain-induced SCs. However, parameters l and L are too small to be measured *in situ*.

Remark 5. When a high-pressure experiment is performed without hydrostatic media, even in nonrotational DAC, the specimen undergoes large plastic deformations.[10,37] This is the case in experiments under megabar pressure, in particular with solid hydrogen.[37] PT conditions for such a case are usually characterized by pressure only and are compared with or led by atomistic calculations of phase equilibrium pressure. Our analysis shows that this is conceptually wrong.

VIII. SUMMARY OF INTERPRETATION OF EXPERIMENTAL PHENOMENA

1. The main nanoscale reason for the reduction of SC pressure due to plastic straining is related to the *strain-induced* rather than pressure- or stress-induced SCs. Strain-induced SC occurs by nucleation on new defects generated by plastic flow. For strong enough defects, *barrierless nucleation* takes place which results in *strain-controlled* rather than time-controlled kinetics. For strain-induced defects of lower potency, *thermal fluctuations* are needed and the contribution of preexisting defects has to be taken into account. This explains the effect of plastic straining on kinetics rather than on thermodynamics for some PT (item I).

Estimates show that for strong defects, *direct SC pressure for the strain-induced SCs can be lower than equilibrium pressure p_e and than the reverse SC pressure under hydrostatic conditions*. This does not mean that plastic straining reduces p_e significantly, because p_e does not appear in any equation for strain-induced nucleation and cannot be determined from the strain-induced experiment. Local pressure in the region of stress concentration near the defect is greater than the p_e (for a given stress deviator). Pressure, averaged over some volume much greater than the nucleus, which is measured in experiments, can be smaller than the p_e. This explains the experimental results mentioned in item 4. SC is promoted by plastic deformation at the pressure above p_ε^d only. Large plastic strain below p_ε^d *suppresses SC* because of strain hardening and growth of K_d. This explains why large plastic deformation during the compression of materials does not cause SC, while relatively small shear strain at relatively high pressure promotes SC significantly.

There is a macroscopic reason why "plastic shear" significantly reduces the pressure for the appearance of the first detectable amount of high-pressure phase in comparison with plastic compression. Despite the fact that in both cases, strain-induced SC in the center of the disk occurs under compression without shear, the *trajectory of the loading in the $\overline{p}$-q plane is very different*. Under compression, pressure grows fast during the deformation process. Under torsion, the pressure is constant. There are several macroscopic reasons why the rotation of an anvil *intensifies the progress of SC* in comparison with the case without rotation. Rotation, significantly reducing the disk thickness, compensates the volume decrease due to SC and increases the pressure in the transforming region. It also increases accumulated plastic strain. If without the rotation of an anvil the material deforms elastically during SC in the central region of the disk, the rotation leads to plastic deformation. This transforms the stress-induced SC to strain-induced SC (which can occur under a much smaller pressure), and also causes significant pressure growth. The effect of rotation is much more pronounced if the high pressure phase is stronger than the parent phase. For CRs, additional macroscopic reasons for intensification may be related to better mixing, fracture, and appearance of "fresh" surfaces.

2. There are two possible reasons for the appearance of "steps" at a pressure distribution. Both of them result in a small τ_r. One of the reasons is related to the flow of the material in the transforming ring to the center of the disk and the formation of the stagnation zone. The second reason is connected to shear stress relaxation due to the TRIP (RIP). The meaning of the value of pressure at the "step" is unclear, but it has nothing to do with p_e.

3. The reduction in pressure hysteresis, Δp, is explained at the *nanoscale* by the fact that pressure for strain-induced direct (reverse) SC is always smaller (larger) than the pressure for stress-induced SC. Because the rotation of an anvil causes more intensive *macroscopic* plastic flow and SC can

occur under constant pressure, the Δp for the case with rotation is smaller than without rotation. However, Δp is not a well-defined characteristic of strain-induced SC. Strain-induced defects may cause simultaneously direct and reverse SC in different regions. It causes the necessity to consider both direct and reverse SC kinetics at the *microscale* and results in the existence of the stationary solution $c_s(p)$. For example, if a system is in the stationary state under any pressure p with corresponding $c=c_s$, then any infinitesimal pressure increase (decrease) followed by plastic straining will cause $1\rightarrow 2$ $(2\rightarrow 1)$ SC, i.e., $\Delta p=0$. This explains experiments in Ref. 16, and demonstrates that the corresponding pressure is not p_e.

4. Plastic strain leads to *strain hardening* and an increase in σ_y, K_d, and K_r, i.e., to an increase of pressure hysteresis for pressure (stress) induced SCs. This explains why plastic straining under conditions which do not cause reverse SC *substitutes reversible SCs with irreversible ones* (item 6). For strain-induced SCs, the growth of K is more than compensated by an increase in the driving force due to the stress concentration at defects generated during plastic flow. That is why pressure hysteresis decreases. So, there is no contradiction between the statements in items 3 and 6. *In item 3, both direct and reverse SCs are strain-induced, while in item 6 only direct SC is strain-induced*.

5. The *pressure self-multiplication* (self-demultiplication) effect is explained by the appearance of phases with the higher (lower) yield stress, see Eq. (36). The necessary conditions for this effect are that the reduction in the thickness of the disk completely compensates the volume decrease due to SCs, and that plastic flow occurs rather than the elastic deformation of the central part of the disk. This is the case for RDAC, as well as for traditional DAC, when SC occurs under a fixed load due to the reduction of σ_y by heating or rotational plastic instability.[10] This is not the case under compression in traditional DAC.

6. Even without plastic deformations, the nonhydrostatic stress state can contribute differently to the driving force X for SC to two alternative phases if they have a different transformation strain deviator. Consequently, the nonhydrostatic stress state can lead to phases which are hidden at the hydrostatic experiment. Plastic straining, due to a change in K and the creation of new stress concentrators, provides many more opportunities for new phases, which not only were not, but cannot be obtained under hydrostatic conditions. This is especially important for the appearance of alternative strong phases. At the *nanoscale*, stress concentration, due to new defects and consequently ΔX, is greater in stronger phase. Let alternative phases 2 and 3 appear as a result of SC from phase 1, and σ_y and elastic moduli of phase 2 (which we designate as "*w*" for weak) be significantly smaller than those of phase 3 ("*s*," strong). For a stronger phase, $K_s>K_w$ (assuming the same L). That is why even if $p_e^{1\rightarrow w}>p_e^{1\rightarrow s}$, it may happen that $p_h^{1\rightarrow w}<p_h^{1\rightarrow s}$. Then the stronger phase cannot be obtained under hydrostatic loading. At the *microscale*, if a stronger phase appears, deformation is more concentrated in the parent phase promoting direct SC. If both strong and weak phases appear, again deformation is more concentrated in a weaker phase which may cause SC $w\rightarrow s$. At the *macroscale*, when in traditional DAC, the material flows to the center of the disk, the material with the smaller σ_y appears in the case without rotation (as pressure is higher at $\sigma_{y1}>\sigma_{y2}$), and the stronger phase will be obtained under compression with rotation (as pressure is higher at $\sigma_{y2}>\sigma_{y1}$). Let the material not flow to the center of the disk with and without rotation. The rotation of an anvil can promote the appearance and growth of the high-strength phase, because rotation transforms stress-induced SC to *strain-induced* SC, and causes significant pressure growth due to the pressure self-multiplication effect during the SC. If alternative phases were known, this means that the plastic straining changes the transformation path (item 12).

7. We see several possible reasons for the increase in rate of strain-induced CR by a factor of 10^2-10^5 compared with liquid-phase CR (item 8). Defects induced by plastic flow create *stress concentration* and a much higher driving force for SC than in liquid at the same macroscopic pressure. Under the same applied force, the *pressure gradient* and a possible pressure self-multiplication effect also create a much higher local pressure in the central part of the disk than in liquid. The *mixing* of components during plastic flow may be comparable with mixing in a liquid phase. For strain-controlled kinetics, $\dot{c}\sim\dot{q}$, which could be *very high* for a thin disk and due to TRIP (RIP). However, it is not clear whether the above reasons are sufficient for the quantitative explanation.

8. A matrix with a yield stress higher (lower) than that for reagents significantly promotes (suppresses) the CRs (item 10), because *plastic strain is concentrated in reacting material (matrix)*. Moreover, the *pressure gradient* and pressure in the central part of the disk is higher (lower) for the stronger (softer) matrix at the same applied load. Note that mixing with ruby particles for pressure measurement may reduce SC pressure.

9. The reduction of SC pressure with the increase of strain rate can be explained by the competition between the product phase nucleation and dislocation slip activation at the defects like dislocation pile-up. For slip, higher τ is necessary for a higher strain rate, which increases τ in Eq. (9). Pressure redistribution at the macroscale may also play a role because of an increase in macroscopic yield stress. Because strain rate grows with the growing radius r, it will lead to a smaller pressure gradient and smaller pressure in the center of the disk. The interplay of these two factors determines the resulting effect of strain rate. For polymers studied in Ref. 8, the independence of c on strain rate may be related to the mutual compensation of both reasons.

10. The regularity in item 14 demonstrates the universal character of strain-induced nucleation at various loading schemes. It allows us to assume that our theory will be applicable to various materials and deformation processes, which occur under static and shock loading, in material synthesis, geophysics, mechanosynthesis, and shear ignition of explosives.

11. The independence of the pressure distribution of rotation of an anvil was obtained in our macroscopic approach using a model of perfectly plastic material. It is definitely not true for hardening or softening material.[35] This, in particular, confirms a postulate about the existence of the limiting surface of the perfect plasticity:[35] above some (rather large)

level of plastic strain, the initially isotropic polycrystalline materials are deformed as perfectly plastic and isotropic with a strain-history-independent limiting surface of the perfect plasticity. This means that the strain hardening is saturated and plastic properties reached their steady state.

12. We can also answer the question why the rotation of the anvil reduces the SC pressure in the center of the disk where plastic shear and shear stresses are absent. Rotation induces significant reduction in thickness and corresponding accumulated plastic strain $q=\ln(h/h_0)$, which according to Eq. (16) induces the SC.

IX. POSSIBLE WAYS TO CONTROL STRUCTURAL CHANGE CONDITIONS

Let us summarize our analysis of various examples as possible ways of controlling SCs by the purposeful control of the thermomechanical loading process and microstructure. These methods (as well as results of items 1 and 3–6 of Sec. VIII) can be used for design of physical experiments with various goals.

1. The trivial contribution of shear stresses to the driving force for SCs is connected with the work of shear stresses along the transformation shear strains. This contribution is extremely important for stress-induced SCs with large γ/ε, e.g., with small volumetric strain ε and large shear γ or uniaxial transformation strain. For example, for martensitic PT in NiTi SMA alloy, $\gamma=0.13$ and $\varepsilon=0.0034$,[43] $\gamma/\varepsilon=38$, which produces the strong effect of shear stress even without pile-up, and magnifies the influence of the pile-up by the factor γ/ε. It may also be important for SC under indentation. When the pressure exceeds the yield stress in shear by a factor of 10–100, like in DAC, the contribution of macroscopic shear stress to the driving force is negligible in comparison with the pressure contribution. However, even in this case, the thermodynamic effect of macroscopic shear stress may be important (a) to choose alternative phases (maybe new phases) or alternative mechanisms which have almost the same ε and different γ (for example, rBN transforms to a zinc-blende structure under hydrostatic and to a wurtzite structure under nonhydrostatic conditions[44]); (b) to choose different martensitic variants (which have the same ε) and microstructure.

2. Shear stress causes the TRIP (RIP). If $\tau=\tau_y$, then traditional plastic flow occurs as well. Both TRIP and traditional plasticity generate defects which serve as nucleation sites for strain-induced SCs. As local, normal, and shear stresses near the strong defect can be higher by a factor of 10–1000 than τ_y, the main nanoscale effect of plastic straining is related to the contribution of local stresses to the driving force. Pure hydrostatic pressure does not cause plastic flow and the appearance of strong stress concentrators, which explains the unique role of shear stresses and strains on SC. Even for $\gamma=0$, Eqs. (9) and (10) exhibit a significant effect of τ on p because of the pressure concentration at the tip of the pile-up.

3. The existence of stationary value c_s (Fig. 8) causes some limitation in the intensification of SCs by plastic straining. A significant amount of high-pressure phase or complete SC can be induced by a large strain at a low pressure for a small M only, i.e., if the kinetics of reverse PT is suppressed or the product phase is much stronger. However, even for a large M, a detectable amount of the product phase can be obtained at a low pressure, which is important for the search of new phases.

4. One aim of controlling the strain-induced SCs, leading to high-pressure phases metastable at ambient pressure, is to decrease K_d and p_ε^d for direct SC and to increase K_r and reduce p_ε^r (or at least p_h^r) below ambient pressure. According to the equation $K=L\varepsilon_0\sigma_y(q)$, preliminary plastic deformation suppresses SCs and increases pressure hysteresis. SCs can be promoted by avoiding plastic straining below p_ε^d (see item 7 below). Annealing at a pressure slightly below p_ε^d will reduce σ_y, K_d, and p_ε^d. Consequently, heating under pressure (or after intermediate unloading) can be used to decrease pressure for the initiation of stress- and strain-induced SCs. Moreover, heavy plastic strain producing high dislocation density inhibits the appearance of new strong stress concentrations such as dislocation piles-ups. Annealing can increase the probability of their generation. Grain growth decreases σ_y (according to Petch-Hall relationship) and increases the maximal length of dislocation pile-up. Reduction of p_h^r and p_ε^r can be achieved by a large plastic deformation of the high-pressure phase at $p>p_\varepsilon^r$ (to avoid strain-induced reverse SC). Another point is to find an unloading path, which minimizes or avoids plastic straining during unloading. Then one has to reduce p_h^r below ambient pressure (rather than to worry about $p_\varepsilon^r>p_h^r$ as well). For example, plastic deformation of the high-pressure phase II of Ge and Si reduced PT pressure to semiconducting phase III.[15] One possible way to reduce plastic strain during unloading is to make unloading as fast as possible (quenching from a high-pressure state).

5. At the large strain of order 0.4 (for rocks) to 1.5 (for metals), according to the regularity revealed in Ref. 35, σ_y and consequently K have to be strain- and strain-history-independent. That is why it is desirable to exceed this strain before SC if one wants to exclude the effect of strain and strain history on σ_y and K. Based on the known data for the strain hardening of metals,[35] the value of K and pressure hysteresis in the maximum hardened state can be higher by a factor of 2–5 than in the annealed state, see also Ref. 24.

6. A thin specimen can be used in a DAC experiment to avoid plastic straining in the central part of the disk during the compression stage. The applied force P has to be smaller than defined by Eq. (22). One of the reasons to use a thin specimen and to avoid plastic straining may be to obtain pressure (stress) induced rather than strain-induced SC even without hydrostatic media. Another reason is to avoid preliminary plastic deformation, which causes a decrease in grain size, strain hardening, and an increase in K; this can reduce SC pressure and pressure hysteresis. For a single crystal, a thin specimen will avoid the formation of a subgrain structure, disorientation of material regions, and will keep the specimen as a single crystal. A very small pressure gradient in the central part of the disk is a signature of elastic deformation rather than plastic flow.

7. Additional axial displacements, compensating volume decrease and causing plastic straining under a fixed load, promote the SC. They can be obtained by (a) reduction of

contact friction in the radial direction due to the rotation of anvils or using some other methods; (b) reduction of yield stress and supporting pressure σ_0 under a fixed applied load, e.g., due to the heating of the whole or external part of a specimen; (c) use of the TRIP (RIP) phenomenon during temperature cycling; and (d) use of rotational plastic instability for highly anisotropic materials. These methods are especially effective for producing high strength materials. They are opposite to the methods in item 6 above, and can also be used to stimulate plastic straining in the center of the disk.

8. Reduction of the dissipative threshold K can be achieved, in addition to the reduction of σ_y (e.g., by annealing) by (a) replacement of *martensitic* PT by *diffusive* PT (Ref. 9); (b) performing SC through a liquid phase.[9,45]

9. A decrease in the energy of internal stresses and consequently an increase in the driving force can be achieved by (a) use of intermediate liquids or materials with a small yield limit; (b) reduction of interface shear strength to promote the semicoherence or incoherence;[9] (c) reduction of interface tensile strength σ_c or use of intermediate materials (layers) around the places of expected nucleation, e.g., brittle materials with small σ_c or without cohesion to the parent phase or liquid;[9] (d) choosing parameters so that solid-solid SC occurs near the melting point. In Ref. 45, we predicted a new phenomenon, namely that solid-solid PT with a relatively large ε_t can occur through virtual melting along the interface at temperatures significantly (more than 100 K) below the melting temperature. Virtual melting represents a new mechanism of stress relaxation and loss of coherency at a moving solid-solid interface. The threshold $K=0$ for this mechanism. Theoretical predictions are in agreement with seven experimental results on the $\beta \rightarrow \delta$ PT in HMX energetic crystal.

10. Macroscopic ways to intensify the SCs include (a) an increase of the axial force after some rotation, i.e., search for a loading $P-\varphi_a$ program (Appendix B); (b) use of cyclic back-forward rotation (Appendix B); (c) use of lateral support (e.g., as in belt-type apparatuses), which will increase σ_o and thickness and, consequently, the volume of the transformed material; (d) increase of deformation rate.

11. For stress-induced SC in a shear band (or surface layer)[3,9,12] and an inclined layer,[9] the following regularities have to be taken into account: (a) Applied shear stresses contribute to the yield condition in a way equivalent to the *decrease* in σ_y, and this is one of the mechanisms of an increase in the driving force for SC; (b) if $\sigma_{y2} \geqslant 2\sigma_{y1}$, τ practically do *not affect* the SC condition; (c) shear stresses can render the SC *impossible*, if due to the necessity of fulfillment of the yield condition for a parent phase, a PT criterion is violated. This is in contrast to experiments in RDAC, where the appearance of a strong phase is promoted. For strain-induced SC, the additional contribution of defects generated during plastic flow has to be taken into account for these problems, e.g., in terms of the strain-controlled kinetics (Sec. V). Even for stress-induced SC, TRIP or RIP produce a strain-induced contribution. Traditional plasticity and RIP (TRIP) can significantly increase temperature, driving force (if it grows with temperature increase), and accelerate the SC kinetics. If the temperature exceeds the melting temperature, then the appearance of a strong phase through melting can be promoted by shear stresses and strains.

12. SC can cause mechanochemical feedback, which can be used to control SC. The pressure self-multiplication (self-demultiplication) effect represents positive (negative) mechanochemical feedback, which promotes (suppresses) SC. RIP and TRIP induce new nucleation sites, which in turn promotes SC (autocatalytic effect). They also increase temperature and represent positive (negative) feedback, if the driving force for SC grows (reduces) with temperature growth. Volume decrease during SC to a high-pressure phase leads to a pressure reduction and negative feedback. This may cause the self-regulation phenomenon, similar to that which we revealed for diamond synthesis.[9] Rotational plastic instability[10] causes positive mechanochemical feedback by intensifying plastic flow, compensating volume decrease due to SC, and by increasing pressure.

13. High pressure allows the plastic straining of materials which are brittle at normal pressure. It also increases the critical stress for dislocation slip. That is why mechanochemical effects may start at some critical pressure and temperature, when SCs is a more preferable relaxation mechanism than fracture and plasticity. Plastic straining creates strong compressive and tensile stress concentrators, which can induce both direct and reverse SCs. In such a way, high pressure can promote SCs to low-pressure phases, as in the case with the PT diamond to graphite.[46]

14. One of the ways to promote (suppress) strain-induced SCs is related to the creation of a microstructure which is favorable (unfavorable) to the appearance of strong defects during plastic deformation. Such a microstructure has to be determined in connection to the mechanism of plastic deformation.

X. CONCLUDING REMARKS

In this paper, continuum physical fundamentals of mechanochemistry were conceptually developed. It is clear that the obtained solutions represent the first approximation only. More detailed FEM solutions of the same problems will be done in the near future. Review of general theory of SC in inelastic materials and typical solved problems (including mechanochemical problems) can be found in Ref. 25. Macroscopic flow theory has to be substituted by continuum and discrete dislocation theories, depending on the scale. The phase field approach[32,47] may give more precise results at the nanoscale and microscale. The atomistic scale has to be considered as well. Also, other loading schemes (e.g., PTs under indentation[46]) have to be analyzed. It is evident that there are a number of mechanisms of strain-induced SCs which were not analyzed in this paper. For example, plastic flow can also facilitate PT due to some dislocation mechanisms of martensite nucleation.[27] We see new perspectives in a combined multiscale experimental and theoretical study of SCs for various materials in terms of the entire stress and plastic strain tensor history rather than the pressure at the beginning of SC. The results can be used to find methods to control and facilitate (or suppress) SCs and to synthesize new materials. In addition, specific physical mechanisms of the creation of

stress concentrators and nucleation sites in specific materials at various spatial scales have to be studied both experimentally and theoretically.

ACKNOWLEDGMENTS

The support for this work was obtained from NSF (CMS-02011108), Texas Tech University, and LANL (C-8060 and 52844). The author is very much indebted to Professor N.V. Novikov, Professor J. Hashemi, Professor Y. Ma, Dr. L. N. Shvedov, and Dr. S. G. Buga for fruitful discussions.

APPENDIX A: DETERMINATION OF THE ANGULAR VELOCITY OF DEFORMED MATERIAL ω

Using Eq. (20), one obtains

$$e_z := -\frac{\partial V_z}{\partial z} = -\frac{\dot{h}}{h}, \quad e_r := -\frac{\partial V_r}{\partial r} = \frac{\dot{h}}{2h},$$

$$e_\theta := -\frac{V_r}{r} = \frac{\dot{h}}{2h} = e_r, \quad \hat{\gamma} := \frac{\partial V_\theta}{\partial z} = \frac{\omega r}{h}. \tag{A1}$$

Here e_z, e_r, and e_θ are normal and $\hat{\gamma}$ is the shear components of the deformation rate tensor. We changed the sign in definition of the normal components of the deformation rate tensor in order to make compressive strains positive. To determine ω, the power balance is used,

$$-P\dot{h} = 2\int_0^R \boldsymbol{\tau}\cdot\boldsymbol{v}(2\pi r dr) + h\int_0^R \sigma_y\dot{q}(2\pi r dr), \tag{A2}$$

combined with Eqs. (22) and (23). Here $\boldsymbol{v}=\{V_r;\omega r/2\}$ is the material velocity at the contact surface (Fig. 9), and the terms on the right-hand side represent the power of shear stresses at two contact surfaces and the plastic dissipation rate D, respectively. Calculations give

$$\boldsymbol{\tau}\cdot\boldsymbol{v} = \frac{\sigma_y}{\sqrt{3}}\frac{\boldsymbol{v}_s}{|\boldsymbol{v}_s|}\cdot\boldsymbol{v} = \frac{\sigma_y r}{2\sqrt{3}}\frac{(\dot{h}/h)^2+\omega^2-\omega\omega_a}{\sqrt{(\dot{h}/h)^2+(\omega-\omega_a)^2}},$$

$$D := \sigma_y\dot{q} = \sigma_y\sqrt{\frac{2}{3}}\sqrt{e_z^2+e_r^2+e_\theta^2+2(\hat{\gamma}/2)^2} = \frac{\sigma_y}{h}\sqrt{\dot{h}^2+\omega^2r^2/3}. \tag{A3}$$

Substituting Eq. (A3) into Eq. (A2), one obtains

$$-P\dot{h} = \frac{2\pi\sigma_y R^3}{3\sqrt{3}}\frac{(\dot{h}/h)^2+\omega^2-\omega\omega_a}{\sqrt{(\dot{h}/h)^2+(\omega-\omega_a)^2}} + \frac{2\pi\sigma_y}{3\omega^2}[3\dot{h}^3+(\dot{h}^2+\omega^2R^2/3)^{3/2}]. \tag{A4}$$

One derives from Eq. (23)

$$\dot{h} = \frac{(\omega-\omega_a)h}{\sqrt{G^2-1}}, \quad G = \frac{h_0}{h} \geqslant 1. \tag{A5}$$

Substituting Eq. (A5), Eq. (22) with $\sigma_0=0$, and $H=h_0$, $\omega = z\omega_a$ $(0\leqslant z\leqslant 1)$ in Eq. (A4), one obtains after some algebra

$$(1.5\sqrt{3}+m)(1-z) = m(1-G^2z) + \frac{3\sqrt{3}(z-1)^3+[3(z-1)^2+(G^2-1)G^2z^2m^2]^{3/2}}{(G^2-1)G^2m^2z^2}, \quad m=\frac{R}{h_0}. \tag{A6}$$

This is a highly nonlinear equation with respect to z depending on the two dimensionless parameters G and m. It is easy to show by constructing a Taylor series about $z=0$ that $z=0$ is one of the solutions of Eq. (A6). This solution corresponds to the absence of material torsion and maximum possible sliding along the contact surface both in circumferential and radial directions. Despite the absence of shear strain due to rotation, compressive strain is maximal for this case. Since experiments exhibit significant material torsion,[19] we will analyze the case $z\neq 0$. We were fortunate to find a very simple approximate solution. In fact, we found the solution for small G $[3(z-1)^2 \gg (G^2-1)G^2z^2m^2]$ and for large G $[3(z-1)^2 \ll (G^2-1)G^2z^2m^2]$, and it appears that the solutions do not differ significantly. Thus, for small and large G, after simplification of the last term, Eq. (A6) has the solutions

$$z_1 = (1+\sqrt{3}G^2m/8)^{-1} \text{ and } z_2 = [1+2m(1-G^2+G\sqrt{G^2-1})/(3\sqrt{3})]^{-1}, \tag{A7}$$

respectively. We will substitute the smallest $G=1$ in the expression for z_1. Numerical analysis of Eq. (A6) shows that z depends weakly on G. The expression for z_2 gives the same three-digit precision for $G=10$ and $G=25$. If we substitute $G=10$ in Eq. (A7) for z_2, we obtain a better agreement with the solution of Eq. (A6) for $G<10$ than by using Eq. (A7) for the variable G. Then instead of Eq. (A7), we obtain $z_1 = 1/(1+0.216m)$ and $z_2 = 1/(1+0.192m)$. The ratio z_1/z_2 varies from 1.08 for $m=10$ to 1.25 for $m\to\infty$. If we assume $z = 0.5(z_1+z_2)$ or $z=1/(1+0.204m)$ and consequently

$$\omega-\omega_a = -\frac{0.204m}{1+0.204m}\omega_a \tag{A8}$$

for any G, the discrepancy with the solution of Eq. (A6) does not exceed 6.125%.

APPENDIX B: SOME WAYS TO INCREASE THE EFFECTIVENESS OF THE ROTATION OF AN ANVIL

As was derived at the end of Sec. VI A, at large anvil rotation φ_a at fixed force, both the shear and compressive plastic strains are small, i.e., rotation is not effective anymore for inducing the SC. To make the rotation effective again, the force P has to be increased. If the rotation stops at some thickness h, the plastic compression can start if the force increases to the value P determined by Eq. (22) with $H=h$ [from the value P_0 determined by Eq. (22) for $h=h_0$]. After the rotation starts, we can again apply Eqs. (21)–(25) starting with $\overline{\varphi}=0$. There are three reasons for the intensification of SCs in this case: larger pressure, larger m, and smaller $\overline{\varphi}$ (consequently larger reduction in thickness). If the rotation starts at force P smaller than necessary for plastic compression, then the new value of h_0 (and m) is determined from Eqs. (22) and (23) and the initial value $\overline{\varphi_0}$ is determined from Eq. (25). The thickness reduction during the rotation can be found from Eq. (25) with $\overline{\varphi}$ calculated from $\overline{\varphi_0}$.

In experiments,[15] sometimes *multiple rotations forward and back* by an angle of order $\varphi_{ai}=5°$ are used. This results in more precise pressure measurement and the repeatability of results due to the smaller effect of the anvil's misalignment for small rotations. The above theory gives the same results for monotonous and forward and back rotation for $\varphi_a=\Sigma|\varphi_{ai}|$. Indeed, if the rotation direction changes, compression does not start before the angle α has reached the same modulus [see Eq. (23)], because the compression under the larger value of τ_r is impossible. There is one possible reason for the higher effectiveness of cycling rotation, which is the difference between plastic behavior for monotonous and nonmonotonous loading. The maximal difference is observed when the stress tensor changes sign. According to the *Bauschienger effect* at a large strain, the yield stress at reverse loading for some metals is two times smaller than for monotonous loading and reaches the same value as for monotonous loading after the strain increment $\Delta q \simeq 0.1$.[35]. A similar effect with a smaller magnitude is observed at any change in the loading direction: the greater the angle between the stress and stress increment vector, the larger the effect is. The only deviatoric component of stress tensor is the shear stress τ. The angle of inclination of τ to the radius changes from α to $-\alpha$, so the angle between shear stress and stress increment vector, $\pi/2+\alpha$, is large enough (for the maximal possible Bauschienger effect, this angle is π). Consequently, the reduction in the yield stress is expected to be at least half of the maximum possible reduction, i.e., of the order $0.25\sigma_y$. The yield stress reaches its initial value after $\Delta q \simeq 0.05$.[35] According to Eq. (22), the thickness will decrease down to a value of order $\Delta q \simeq 0.05$, necessary to reach the initial value of σ_y. A similar phenomenon occurs for plastic contact friction.[35] Consequently, forward and back rotation with small φ_{ai} leads to a *more intensive thickness reduction, straining, and SC*. This result has to be checked quantitatively by experiments.

*Email address: valery.levitas@coe.ttu.edu; Fax: (253) 679 8926.

[1] H. W. Green and P. C. Burnley, Nature (London) **341**, 733 (1989).

[2] C. S. Coffey and J. Sharma, in *Proceedings of the 11th International Detonation Symposium, Colorado, 2001* (Naval Research Office, Arlington, 2001), p. 751.

[3] V. I. Levitas, V. F. Nesterenko, and M. A. Meyers, Acta Mater. **46**, 5929 (1998).

[4] C. C. Koch, Nanostruct. Mater. **2**, 109 (1993).

[5] M. A. Grinfeld, J. Nonlinear Sci. **3**, 35 (1993).

[6] J. J. Gilman, Science **274**, 65 (1996); Philos. Mag. B **71**, 1057 (1995).

[7] A. N. Dremin and O. N. Bruesov, Russ. Chem. Rev. **37**, 392 (1968); N. N. Thadhani, R. A. Graham, T. Royal, E. Dunbar, M. U. Anderson, and G. T. Holman, J. Appl. Phys. **82**, 1113 (1997); A.I. Rusanov, Russ. J. Gen. Chem. **70**, 138 (2000).

[8] A. A. Zharov, Usp. Khim. **53**, 236 (1984); *High Pressure Science and Technology, Proceedings of the XI AIRAPT International Conference*, edited by N. V. Novikov (Naukova Dumka, Kiev, 1989), Vol. 1, p. 377; in *High Pressure Chemistry and Physics of Polymers*, edited by A. L. Kovarskii (CRC Press, Boca Raton, FL, 1994), Chap. 7, pp. 267–301.

[9] V. I. Levitas, J. Mech. Phys. Solids **45**, 923 (1997); **45**, 1203 (1997).

[10] V. I. Levitas and L. K. Shvedov, Phys. Rev. B **65**, 104109 (2002).

[11] N. V. Novikov, I. A. Petrusha, L. K. Shvedov, S. B. Polotnyak, S. N. Dub, and S. A. Shevchenko, Diamond Relat. Mater. **8**, 361 (1999).

[12] V. I. Levitas, Int. J. Solids Struct. **35**, 889 (1998); Int. J. Plast. **16**, 805 (2000); **16**, 851 (2000).

[13] P. W. Bridgman, Phys. Rev. **48**, 825 (1935); Proc. Am. Acad. Arts Sci. **71**, 387 (1937); *Studies in Large Plastic Flow and Fracture* (McGraw-Hill, New York, 1952); N. S. Enikolopyan, Pure Appl. Chem. **57**, 1707 (1985); Russ. J. Phys. Chem. **63**, 1261 (1989).

[14] L. F. Vereschagin, E. V. Zubova, K. P. Burdina, and G. L. Aparnikov, Dokl. Akad. Nauk SSSR **196**, 81 (1971).

[15] M. Aleksandrova, V. D. Blank, A. E. Golobokov, Yu. S. Konyaev, and E. I. Estrin, Solid State Phys. **29**, 2573 (1987); M. M. Alexandrova, V. D. Blank, A. E. Golobokov, and Yu. S. Konyaev, *ibid.* **30**, 577 (1988); M. M. Alexandrova, V. D. Blank, and S. G. Buga, *ibid.* **35**, 1308 (1993).

[16] V. D. Blank, Yu. Ya. Boguslavski, M. I. Eremetz, E. S. Izkevich, Yu. S. Konyaev, A. M. Shirokov, and E. I. Estrin, JETP Lett. **87**, 922 (1984); Phys. Lett. A **188**, 281 (1994).

[17] V. D. Blank, G. A. Dubitsky, and S. A. Plotyanskaya, in *High Pressure Science and Technology*, edited by W. A. Trzeciakowski Proceedings of the Joint XV AIRAPT and XXXIII EHPRG International Conference, Warsaw, 1995 (World Scientific, London, 1995), pp. 325–327.

[18] V. D. Blank, Z. H. Malyushitska, and B. A. Kulnitskiy, High Press. Phys. Eng. **3**, 28 (1993).

[19] S. G. Buga and V. D. Blank, High Press. Phys. Eng. **3**, 40 (1993).

[20] N. V. Novikov, S. B. Polotnyak, L. K. Shvedov, and V. I. Levitas, Superhard Mater. **3**, 39 (1999); N. V. Novikov, L. K. Shvedov,

V. I. Levitas, I. A. Petrusha, and S. B. Polotnyak, in *Synthesis, Sintering and Properties of Superhard Materials*, edited by A. A. Shulzhenko (Institute for Superhard Materials, Kiev, 2000), pp. 131–144.

[21] V. I. Levitas, J. Hashemi, W. Mathis, M. Holtz, and Y. Ma, *Brookhaven National Laboratory Year Book* (2002); Y. Ma, V. I. Levitas, J. Hashemi, W. Mathis, and M. Holtz, *Brookhaven National Laboratory Year Book* (2002); V. I. Levitas, J. Hashemi, and Y. Ma, Europhys. Lett. **68**, 250 (2004).

[22] F. Dachille and R. Roy, *Modern High Pressure Technique* (Mir, Moscow, 1964), pp. 256–283.

[23] N. R. Serebryanaya, V. D. Blank, and V. A. Ivdenko, Phys. Lett. A **197**, 63 (1995).

[24] V. D. Blank, Y. S. Konyaev, V. T. Osipova, and E. I. Estrin, Inorg. Mater. **19**, 72 (1983); E. I. Estrin, *Phase Transformation of Martensitic Type*, edited by V. V. Nemoshkalenko (Naukova Dumka, Kiev, 1993), pp. 110–139.

[25] V.I. Levitas, *Continuum Mechanical Fundamentals of Mechanochemistry*, in *High Pressure Surface Science and Engineering*, edited by Y. Gogotsi and V. Domnich (Institute of Physics, Bristol, 2004), pp. 159–292.

[26] E. K. H. Salje, *Phase Transitions in Ferroelastic and Co-Elastic Crystals* (Cambridge University Press, New York, 1990).

[27] G. B. Olson and M. Cohen, J. Less-Common Met. **28**, 107 (1972); Metall. Trans. A **6A**, 791 (1975); *Dislocations in Solids*, edited by F. Nabarro (Elsevier, Amsterdam, 1986), Vol. 7, pp. 297–407; G. B. Olson, in *Deformation, Processing and Structure*, edited by G. Krauss (ASM International, Warrendale, PA, 1984), pp. 391–424.

[28] V. I. Levitas, A. V. Idesman, and E. Stein, Int. J. Solids Struct. **35**, 855 (1998); A. V. Idesman, V. I. Levitas, and E. Stein, Comput. Methods Appl. Mech. Eng. **173**, 71 (1999); Int. J. Plast. **16**, 893 (2000).

[29] V. I. Levitas, A. V. Idesman, and G. B. Olson, Acta Mater. **47**, 219 (1999).

[30] V. I. Levitas, A. V. Idesman, G. B. Olson, and E. Stein, Philos. Mag. A **82**, 429 (2002).

[31] J. P. Hirth and J. Lothe, *Theory of Dislocations* (Krieger, Malabar, FL, 1992).

[32] G. B. Olson and A. L. Roytburd, in *Martensite*, edited by G. B. Olson and W. S. Owen (ASM International, Materials Park, OH, 1992), Chap. 9, pp. 149–174; A. C. E. Reid, G. B. Olson, and B. Moran, Phase Transitions **69**, 309 (1998).

[33] M. A. Meyers, O. Vohringer, and V. A. Lubarda, Acta Mater. **49**, 4025 (2001).

[34] T. Mura, *Micromechanics of Defects in Solids* (Martinus Nijhoff Publishers, Dordrecht, 1987).

[35] V. I. Levitas, *Large Deformation of Materials with Complex Rheological Properties at Normal and High Pressure* (Nova Science Publishers, New York, 1996).

[36] J. Lubliner, *Plasticity Theory* (Macmillan Publ. Comp., New York, 1990).

[37] A. F. Goncharov, E. Gregoryanz, R. J. Hemley, and H. K. Mao, Proc. Natl. Acad. Sci. U.S.A. **98**, 14 234 (2001); P. Loubeyre, F. Occelli, and R. LeToullec, Nature (London) **416**, 613 (2002); C. Narayana, H. Luo, J. Orloff, and A. L. Ruoff, *ibid.* **393**, 46 (1998).

[38] V. I. Levitas, S. B. Polotnyak, and A. V. Idesman, Strength Mater. **3**, 221 (1996); S. Merkel, R. J. Hemley, and H. K. Mao, Appl. Phys. Lett. **74**, 656 (1999); W. C. Moss, J. O. Hallquist, R. Reichlin, K. A. Goettel, and S. Martin, *ibid.* **48**, 1258 (1986); N. V. Novikov, V. I. Levitas, S. B. Polotnyak, and M. M. Potyomkin, High Press. Res. **8**, 507 (1991); N. V. Novikov, V. I. Levitas, S. B. Polotnyak, and M. M. Potyomkin, Strength Mater. **26**, 64 (1994).

[39] P. Ogibalov and I. Kiyko, *Notes on High Parameters Mechanics* (Moscow University, Moscow, 1962).

[40] V. F. Zackay, E. R. Parker, D. Fahr, and R. Busch, Trans. ASM **7**, 252 (1967); K. A. Padmanabhan and G. J. Dabies, *Superplasticity* (Springer-Verlag, Berlin, 1980).

[41] V. D. Blank, Yu. Ya. Boguslavski, S. G. Buga, E. S. Itskevich, Yu. S. Konyaev, and A. M. Shirokov, *High Pressure Science and Technology, Proceedings of the XI AIRAPT International Conference*, edited by N. V. Novikov (Naukova Dumka, Kiev, 1989), Vol. 4, pp. 64–66.

[42] R. J. Hemley, H. K. Mao, G. Shen, J. Bardo, Ph. Gillet, M. Hanfland, and D. Häusermann, Science **276**, 1242 (1997).

[43] K. Jacobus, H. Sehitoglu, and M. Balzer, Metall. Mater. Trans. A **27**, 3066 (1996).

[44] V. F. Britun and A. V. Kurdyumov, High Press. Res. **17**, 101 (2000).

[45] V. I. Levitas, B. F. Henson, L. B. Smilowitz, and B. W. Asay, Phys. Rev. Lett. **92**, 235702 (2004).

[46] Y. G. Gogotsi, A. Kailer, and K. G. Nickel, Nature (London) **401**, 663 (1999).

[47] V. I. Levitas and D. L. Preston, Phys. Rev. B **66**, 134206 (2002); **66**, 134207 (2002); V. I. Levitas, D. L. Preston, and D-W. Lee, *ibid.* **68**, 134201 (2003); A. A. Boulbitch and P. Toledano, Phys. Rev. Lett. **81**, 838 (1998); V. I. Levitas, A. V. Idesman, and D. L. Preston, *ibid.* **93**, 105701 (2004).